Journal of Theoretical and Applied Information Technology
31st March 2025. Vol.103. No.6

ISSN: 1992-8645 www.jatit.org E-ISSN: 1817-3195

AI BASED MODIFIED APPROACH IN HIGH-RESOLUTION IMAGE RESTORATION TECHNIQUES FOR SMART HEALTHCARE SYSTEM: A TECHNICAL REVIEW AND ANALYSIS

PRASANTA KUMAR SAHOO[1], DEBASIS GOUNTIA[2], RANJAN KUMAR DASH[3], MANAS KUMAR NANDA[4*]

[1]PhD Research Scholar, RIA Laboratory, School of Computer Sciences, Odisha University of Technology and Research Bhubaneswar-751029, Odisha, India
[2]Associate Professor, School of Computer Sciences, Odisha University of Technology and Research Bhubaneswar-751029, Odisha, India
[3]Professor and Head, School of Computer Sciences, Odisha University of Technology and Research Bhubaneswar-751029, Odisha, India
[4*]Assistant Professor, Dept. of Computer Applications, ITER, SOA University, Bhubaneswar-751030, Odisha, India
E-mail: [1]mrprasantasahoo@gmail.com, [2]dgountia@outr.ac.in, dgountia@cs.iitr.ac.in , [3]rkdash@outr.ac.in, [4*]manasnanda@soa.ac.in

ABSTRACT

Medical image analysis is the most prominent research area of digital image processing. In digital image processing, medical images are more sensitive and informative. Data loss in medical image processing harms patients and the healthcare system. Therefore, several medical image analysis techniques play a significant role in ensuring lossless information during disease diagnosis. The visual clarity of an image depends upon its high resolution. Therefore, high resolution is crucial in medical image analysis. The high-resolution problem occurs due to spatial resolution limitations. These limitations can be attributed to hardware limitations, low radioactivity doses, or the acquisition time of a specific image. To avoid these limitations, several high-resolution image restoration (or reformation) techniques are available. These techniques include image compression, histogram equalization, edge detection, feature extraction, image synthesis, and noise reduction, among others. Recently, different AI-based techniques, like machine learning (ML) and deep learning (DL), have been considered booming technologies for high-resolution image reformation. Therefore, we felt it was necessary to review various AI learning-based techniques and their applications in the reformation of high-resolution digital images. The digital images may include various types, such as medical images or those from the Indian Historical Society. In this article, we first shed light on different modalities of medical image analysis techniques with their image acquisition properties. We then apply machine learning and deep learning AI approaches to the image acquisition properties to address the issue of poor visual quality in the images. This serves as evidence that ML and DL models must modify the component configuration of medical image modalities to reform high-resolution images. To improve the quality of low-resolution images, we are building new models for histogram equalization, compression, decompression, and noise reduction based on this comprehensive review.

Keywords: *High-Resolution, Image Enhancement, Medical Image Analysis, Image Compression, Machine Learning, Deep Learning.*

1. INTRODUCTION

To help with the reformation of high-resolution images, this review work will give a general outline of the AI model's structure and explain what threshold functions are, how they work, and any limitations they may have. Moreover, we have mentioned detail the effects of noise in order to build high-resolution images. The input images are may be of single image based or multi-image-based inputs, depends on configuration of medical image modalities. When working with images as an input, we can classify their pixel values and edges as low-level features; texture and motif are examples of mid-level features; and object parts and objects themselves are examples of high-level features. In order to identify the most relevant works and any gaps in their coverage, we used the PRISMA 2020 model for conducting a critical literature review.

1.1 High Resolution in Medical Imaging System

The main aim of electronic imaging applications is to acquire high-resolution (HR) images. HR is defined as having a high pixel density within an image. In various critical applications, HR images provide more detailed information. Therefore, HR medical images are more supportive for physicians to make accurate diagnoses [1]. The HR satellite images are also more useful in distinguishing from other, more similar objects [2]. Providing HR images in computer vision will enhance pattern recognition performance. For digital image acquisition, charge-coupled devices (CCD) and complementary metal oxide semiconductor (CMOS) sensors have been used widely since the 1970s. Although both sensors are generally suitable for the analysis of medical images, the existing level of resolution and consumer price will not fulfil the forthcoming mandate. For example, consumers always want low-priced HR digital cameras or camcorders, whereas scientists always need HR-level digital cameras close to 35 mm film, which have no visible artifacts when an image is magnified. Therefore, there is a need for improvement in the current resolution level. So, to increase the HR level, there may be two solutions, i.e., increasing spatial resolution by reducing the size of the pixel or increasing spatial resolution by enhancing the size of the chip [3].

The most general method to increase HR level is pixel size reduction, i.e., the per-unit area number of pixels will be increased using sensor manufacturing methods. Since pixel size decreases, the existing light also decreases. Consequently, a short noise issue arises, significantly reducing the lighting quality. Therefore, if we reduce the pixel size without encountering a short noise issue, the reduction is limited to about 40 mm^2 for a 0.35 mm CMOS process. Almost all current sensor technology has achieved this level [4].

The second approach increases the spatial resolution by enhancing chip size, leading to a corresponding increase in capacitance. However, large capacitance makes it difficult to speed up a charge transfer rate that is not an effective one. Given the high cost of precession cameras, the image sensor plays a crucial role in many commercial applications related to HR imaging, particularly in signal processing and hardware setup. So, it is not in the scope of our review process. Therefore, in our review process, we resize the pixel to construct HR images [5].

HR imaging algorithms may be categorized depending on the number of input and output images intricately involved in the process of digital image analysis. In this article, we focused on the high-resolution (HR) images that will be recovered from low-resolution (LR) images using some existing artificial intelligence models, such as machine learning (ML) and deep learning (DL) models. Since these existing models are ill-posed inverse problems, even slight changes in the effect can lead to drastic changes in the underlying causes. To avoid the inverse ill-posed problems, the existing DL models are used for optimization techniques. So, we decide to write some artificial intelligence algorithms or models rather than existing ill-posed DL models [6-13].

1.2 Deep Learning in Medical Imaging System

Deep learning is the most promising AI technique for digital image processing. It can perform various image-processing tasks. For instance, it is capable of performing various image-processing tasks such as image classification [14], image denoising [6], image segmentation [7], object detection, and solving inverse problems [16]. It offers two advantages over other models used for image processing. The first one is well-developed parallel calculation, and the second one is powerful representation capability.

The existing DL framework has been developed using an artificial neural network. Several neural net models, including Caffe [17], MaxNet [18], TensorFlow [19], and others, facilitate parallel calculations. The users get direct benefits in high-speed parallel computations without using GPU architecture and low-level GPU programming. The diagram below illustrates the structure of a neural network deep learning framework.

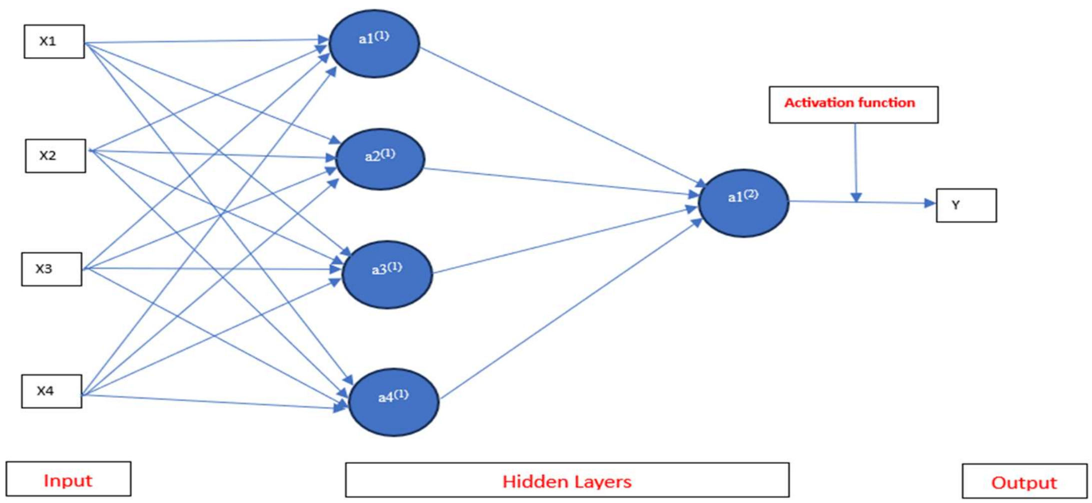

Figure 1: Structure of classical neural network.

In Figure 1, both of the input-output external layers are linked to training data. An activation function, which is a user-selected mathematical function, makes the network stronger. A neuron, consisting of a linear transformation and a non-linear activation function, represents each solid circle.

DL helps process data with high-level features. Although the efficiency of DL can be judged by the amount of data, implicit information of large quantity parameters is also revealed by DL networks. On the contrary, we can say that a restricted number of data restricts its performance.

1.2.1 Neural net units

The DL model consists of multiple neural network layers. We broadly classify the entire multi-layer neuron network into three layers. For the layers from left to right, the 1st layer is called the input layer or outer layer, and the last layer is called the output layer, and the layers present within the 1st layer and the last layer, any number of layers, are called hidden layers or middle layers, as shown in Fig. 1, which is a classical DL model network with hidden layers. Neurons are shown in this model as solid circles, and each one is made up of a linear transformation and a non-linear point-wise activation function [20].

1. Linear transformation

The multi-layer neural network consists of multiple layers and multiple neurons. Each neuron at layer L is connected to all neurons at its successive layer L+1 through a connecting sensor line/Channel having weight $W_{i,j}^{L}$ L L € R, where i is the neuron index at layer L and j is the neuron index at layer L+1 and the weight matrix $W^{L} \in \mathbb{R}^{C^{L+1} \times C^{L}}$, here C^L is the channel at layer L and C^{L+1} is the channel at Layer L+1. Let the output produced at layer L be O^L and $O^{L} \in \mathbb{R}^{C^{L \times M \times N}}$, where M is the height and N is the width of the image. Let σ^L be the activation function at layer L. So, the output at layer L+1 is O^{L+1} is defined as,

$$O^{L+1} = \sigma^{L}(W^{L} \times O^{L}) \qquad (1)$$

Here the multiplication operation between $W^{L}\ and\ O^{L}$ is the linear matrix multiplication operation. But the point to be noted here is that width and height of image will not be alter. When the above liner operation is convolution, $W_{i,j}^{L}\ becomes\ a\ convolution\ filter$ and the neural net becomes a Convolutional Neural Network (CNN) [29].

2. Activation functions

Activation functions are used in neural networks to check whether a neuron is active or not. When a neuron is active, mathematical operations use its input to make predictions. The main role of the activation function is to produce output from a set of input values fed to the node or layer, and activation functions are needed for neural networks since activation functions help to introduce nonlinearity to the neural network. Some of the most widely used activation functions are defined as follows [30].

Journal of Theoretical and Applied Information Technology
31st March 2025. Vol.103. No.6

ISSN: 1992-8645 www.jatit.org E-ISSN: 1817-3195

a. Binary step activation function

This activation function acts on a threshold value. The threshold value is a predefined cut-off value, which tells about whether a neuron is activated or not. i.e., the input fed to the neuron through the activation function at the input layer will be compared to the predefined threshold value; if it is greater, then the neuron is activated; otherwise, the neuron is deactivated, which is mathematically defined as:

$$f(x) = \begin{cases} 0, & x < 0 \\ 1, & x \geq 0 \end{cases} \qquad (2)$$

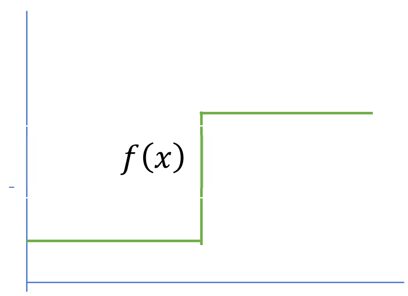

Figure 2: Binary Step Activation Function

Limitations:

1. It is unable to process multi-class classification problems.

2. Due to the gradient value being zero, it creates an interruption in the back propagation process.

b. Linear activation function

This activation function is proportional to the neuron's input at each layer. Therefore, it is also known as the identity function. This function does not alter the weighted sum of the input; instead, it divides the input values into two groups. Which is mathematically defined as:

$$f(x) = mx + b \qquad (3)$$

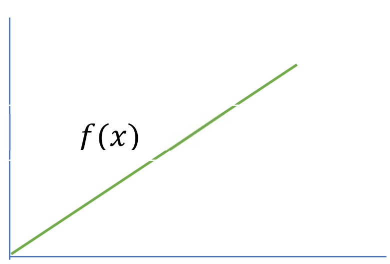

Figure 3: Linear Activation Function

Limitations:

1. This function has no relation to input x of any neuron since it is a constant function.

2. In a neural network, if a linear activation function is used, there is no meaning of multiple layers because the last layer will still linearly function of 1st layer. So linear function converts multiple layers into a single layer.

c. Sigmoid or logistic activation function

This activation function ranges from real number 0.0 to real number 1.0. So, the value having 1.0 is considered a larger input value or a more positive value, and the value having more negative numbers is considered a smaller input value; the output value will be closer to 0.0, so it is shaped into an S-shape, which is mathematically defined as:

$$f(x) = \frac{1}{1 + e^{-x}} \qquad (4)$$

Figure 4: Sigmoid or Logistic Activation Function

Limitations:

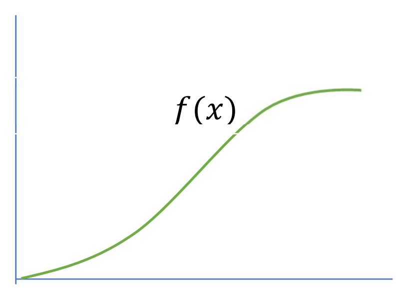

1. Training of the neural network is more difficult and unstable due to the function is not symmetric around zero, so the output produced by all neurons is of the same sign.

d. Tanh function/ hyperbolic tangent function

The Tanh activation function is the same functionally and in S-shape as the sigmoid/logistic activation function, but the Tanh activation function is different in output range from -1 to 1. In Tanh, if the input value is more positive or larger, then the output value will be closer to 1.0, but in case the input value is more negative or a smaller value, then the output value will be closer to -1.0, which is mathematically defined as:

ISSN: 1992-8645 www.jatit.org E-ISSN: 1817-3195

$$f(x) = \frac{(e^x - e^{-x})}{(e^x + e^x)} \qquad (5)$$

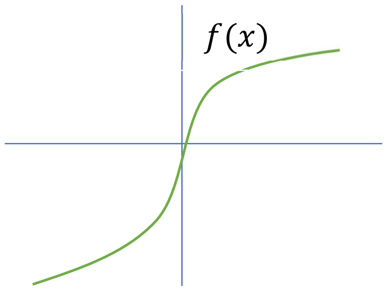

Figure 5: Tanh Function/ Hyperbolic tangent function

Limitations:

1. Like the Sigmoid function Tanh function also suffers from the problem of Vanishing gradients.

2. Compared to the sigmoid function, the Tanh function gradient value is much steeper or sharper.

e. Rectified linear unit (ReLU) function

This function is linear. ReLU facilitates backpropagation and enhances computation efficiency by simultaneously activating only a specific number of neurons. Due to its more convergent gradient descent and non-saturating properties, it aids in the global minimization of the loss function. It is mathematically defined as:

$$f(x) = \max(0, x) \qquad (6)$$

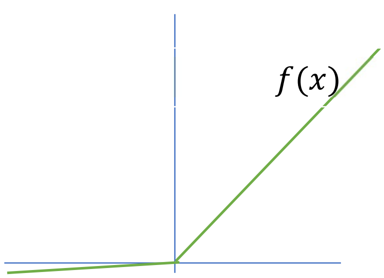

Figure 6: Rectified Linear Unit (ReLU) Function

Limitations:

1. It suffers from the Dying ReLU problem, i.e., due to negative input values, the gradient value becomes zero, so in the back propagation process, some neuron's weight and bias values are not updated. So, neurons never get activated,

2. Due to the Dying ReLU problem model's ability decreases.

f. Leaky ReLU (LReLU) function

This function has a small positive slope on the negative area. So, this function is an improved form of the ReLU function. Hence, it circumvents the issue of the ReLU function dying. Therefore, the Leaky ReLU function has the ability to activate neurons during the backpropagation process of the neural network model. It is mathematically defined as:

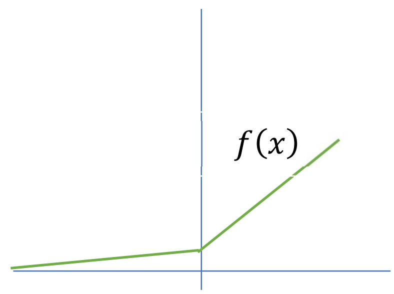

$$f(x) = \max(0.1x, x) \qquad (7)$$

Figure 7: Leaky ReLU (LReLU) Function

Limitations:

1. For Negative input values, prediction is not consistent.

2. Learning model parameters is time-consuming due to the small gradient value for negative input values.

g. Parametric ReLU (PReLU) function

This function is another variant of the Rectified Linear Unit (ReLU) function; it is generally used to solve the Dying ReLU problem of the negative value part of the axis. To find out the slope of the negative part of the axis, this function takes a parameter, say 'a,' which is called a negative values slope parameter. So, during the backpropagation process, parameter 'a' helps to learn the appropriate value. It is mathematically defined as:

$$f(x) = \max(ax, x) \qquad (8)$$

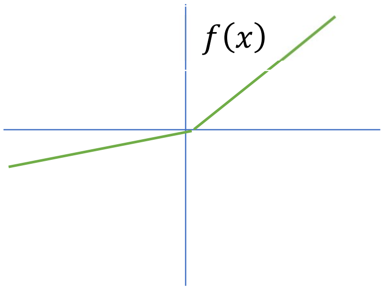

Figure 8: Parametric ReLU (PReLU) Function

Limitations:

1. Unable to activate dead neuron, i.e., the relevant information is not passed successfully, to the next layer neurons.

2. It provides non-uniform value for different problems, as it depends upon slope parameter value 'a'.

h. Exponential linear units (ELUs) function

This function is also another variant of the ReLU function. Generally, one uses it to modify the slope of a function's negative part. It uses the log curve instead of parameter values like LReLU and PReLU functions to solve the Dying ReLU problem in the negative value part of the axis. It is mathematically defined as:

$$f(x) = \begin{cases} x, & x \geq 0 \\ \alpha\,(e^{x} - 1), & x < 0 \end{cases} \quad (9)$$

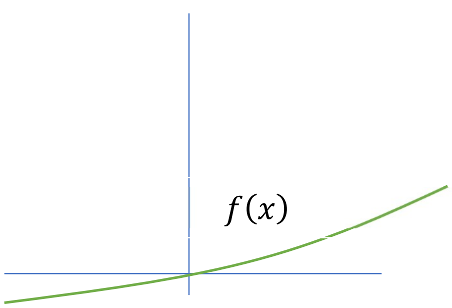

Figure 9: Exponential Linear Units (ELUs) Function

Limitations:

1. Computational time is very high due to the inclusion of exponential operation.

2. *No Learning of the α value*

takes place.

3. Gradient problem Explosion.

i. Scaled exponential linear units (SELUs) function:

This function is a variant of the ELUs function. It is a self-normalizing activation function. Due to the self-normalization property, there is no need for the inclusion of batch-normalization layers. Therefore, it ensures consistent output standardization. It is mathematically defined as:

$$f(x) = \begin{cases} \lambda\, x, & x > 0 \\ \lambda\alpha(e^{x} - 1), & x \leq 0 \end{cases} \quad (10)$$

Here $\boldsymbol{\lambda}$ and $\boldsymbol{\alpha}$ are constants having values $\boldsymbol{\lambda} \cong 1.0505$ and $\boldsymbol{\alpha} \cong 1.6732$

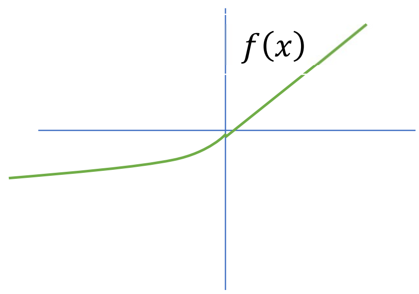

Figure 10: Scaled Exponential Linear Units (SELUs) Function

Limitations:

1. Computational time is very high due to the inclusion of exponential operation over negative values.

2. Positive input values are linearly presented.

The graphical representation of the above-discussed activation functions is shown below:

1.2.2 Deep learning in high resolution

In deep learning, there are two distinct methods for constructing high-resolution images from low-resolution images, such as the single-image high-resolution method and the multi-image high-resolution method. The multi-image-based method combines subpixel-shifting in low-resolution images with information from higher-resolution images to create new ones. This process gives the new ones more accuracy. Typically, we use the multi-image method to establish global or local photometric relationships between multiple low-resolution images. Some examples of multi-image-based high-resolution image reconstruction methods are interpolation-based methods [21], frequency domain-based methods [21], regularization-based methods [22, 23], etc. There are few deep learning models applied over multi-image low-resolution problems to construct high-resolution images [24]. A lot of the authors of multi-image-based high-resolution models have used deep residual networks to make the results better in multiple satellite images. However, residual networks may not work well with medical images because they lose information. There are many deep learning models available to construct high-resolution images from low-resolution images using single-image-based methods, especially in medical image analysis, whose formulation details are given below.

1.2.2.1 Single-image-based high-resolution method

Let G is the set of low-resolution images and F is the set of high-resolution images. Select a single image g from G such as that g ϵ G and a newly constructed high-resolution image f such as that f ϵ F. The high-resolution forward problem can be stated as

$$g = Af \qquad (11)$$

Here, A is the contaminated particle operand that includes noise, blur, or down-sampling operation and is defined as A: X → Y. For a given set of training datasets (g_i, f_i), we aim to find out A' such that prediction value $f' = A'g \text{ so that } f \approx f'$. Let's consider L is a user choice loss function to minimize the parameters of the network and A' is the parametric approximate inverse operator and mapping from $A'_\theta : Y \rightarrow X$ *is learned by solving the equation*

$$\underset{\theta \in \ominus}{\arg\min} \sum L\left(f_i', A'_\theta(g_i)\right) + R(\theta) \qquad (12)$$

$here\ \ominus\ is\ the\ set\ of\ possible\ parameters$

$and\ R(\theta)\ is\ the\ regularization\ function$

Construction of high-resolution images from low-resolution images using deep learning has been broadly discussed in li literature reviews [2, 9, 10, 24, 12, 25, 26, 27, 11]. Although we have reviewed many more networks for high resolution, it is not possible to present exclusively all the networks. So, we selected some sets of these techniques and planned the implementation of deep learning in high-resolution issues.

1.2.2.2 Formulation of estimation metrics and cost functions

The cost functions are generally realized in the form of evaluation metrics and it is used for model optimization. The Peak-Signal-to-Noise Ratio (PSNR) is mostly used for the measurement of the quality of reconstructed metrics in case of high resolution or super-resolution. The evaluation of PSNR depends upon Mean Square Error (MSE). The MSE is called the L_2 loss function and it is defined as a difference at pixel level. The MSE and PSNR are formulated as follows [3, 28].

$$PSNR = 10 \times log_{10}\left(\frac{MAX_I^2}{MSE}\right)$$
$$=20 \times log_{10}\left(\frac{MAX_I}{\sqrt{MSE}}\right)$$
$$=20 \times log_{10}(MAX_I) - 10 \times log_{10}(MSE) \qquad (13)$$

here

MAX_I=255, i.e., Maximum Possible Pixel value of the image uint8 or 8-bit per pixel.
MSE= Mean Square Error and

$$MSE = \frac{1}{m \times n}\sum_{i=0}^{m-1}\sum_{j=0}^{n-1}[LR(i,j) - HR(i,j)]^2 \qquad (14)$$

Here,
m x n = Dimension of Image
$LR(i,j)$= Ground truth Image
$HR(i,j)$ =Reconstructed Image

1.3 Medical Image Analysis

Medical image analysis or medical imaging or radiology is a technique through which physicians will take the acquisition of images of the interior part of a body for various clinical diagnoses, medical intrusion, and also for visualization of the functionalities of some organs or tissues. There are different modalities are available for medical image acquisitions such as Magnetic Resonance Imaging (MRI), Computed Tomography (CT) Scan imaging, Ultrasound Imaging, X-ray Imaging, and some nuclear medicine imaging [31].

ISSN: 1992-8645 www.jatit.org E-ISSN: 1817-3195

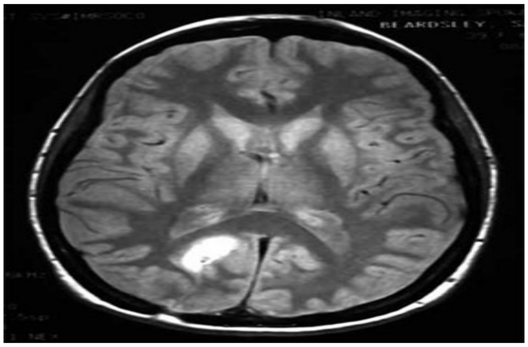

Figure 11: MRI Image of Brain Tumour [Wikipedia]

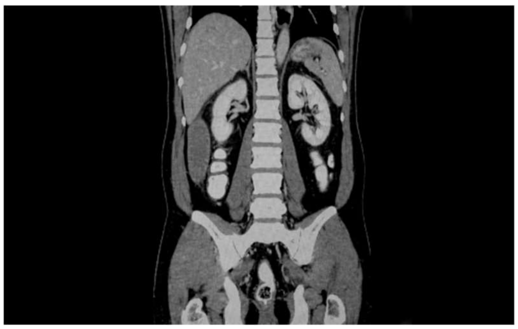

Figure 12: CT scan Images of abdomen-Pelvis body [Wikipedia]

Figure 13: Ultra Sound Image of Baby [Wikipedia]

Figure 14: X-ray Image of Chest [Wikipedia]

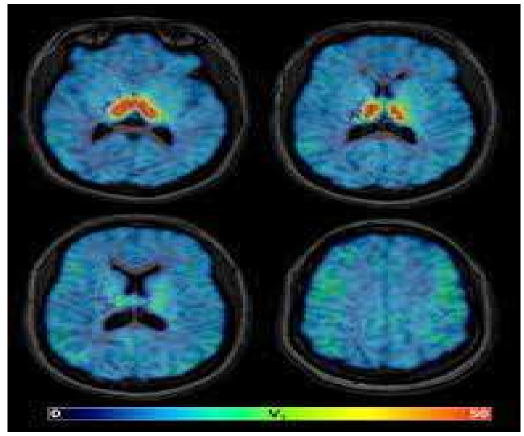

Figure 15: Study of aging Brain using nuclear medicine [medicalexpress.com]

2 PROBLEM STATEMENT

We intended to develop an algorithm or artificial model after the literature study. That algorithm can restore or reform a high-resolution image. We will create a modified compression algorithm to transform low-resolution images into high-resolution ones. This algorithm has numerous potential applications in the field of information security, including but not limited to digital image watermarking, data encryption and decryption, and high-resolution image reformation.

We will compare our work to various existing machine-learning models, as shown in Table 3, based on the Peak Signal Noise Ratio (PSNR), Mean Square Error (MSE), and Structural Similarity(SSIM) Index values and many mores..

3 RESEARCH METHODOLOGY

This section presents different protocols that help to detect, collect, and evaluate the up-to-date techniques used for medical image analysis in this review study. It has been divided into 4-phases, i.e., research questionnaires, strategies of research, article choice norms, and research outcomes [32].

3.1 Research Questionnaires

The aim of a Systematic Literature Review (SLR) is to respond to possible research questions and find out what research outcomes from previously used a new era of design, technology, safety, innovation, comfort, and performance of research results. The research questions are again sub-divided into 5-questions:

Q1: What are the different modalities of medical image processing or medical imaging?
Q2: Why medical image processing and analysis?
Q3: Which medical image processing technique is suitable for a high-resolution image reconstruction system?
Q4: Which high-resolution image reconstruction method has been implemented and adopted?
Q5: Has the developed method produced good results?
We performed the relevant systematic review study from several databases such as Taylor & Francis, IEEE Explorer, Google Scholar, Springer and Elsevier, and many more. During the systematic review, we mainly focused on two or more questions from the proposed research questionnaires.

3.2 Research Tactic and Flow Diagrams of Article Selection Procedure

In this section, we discussed the procedure and protocols of article selection and rejection. The Fig. 16 represents details of the literature review, i.e., article collections, article selection, and article rejection criteria. Fig. 17 represents the overall systematic review of articles.

Our literature review was performed systematically over several databases like SCI, Scopus, IEEE Explorer, Google Scholar, Springer Elsevier, and many more. We used collections of several keywords and terminologies like "Medical Image Processing", "Medical Image Processing Techniques", "Medical Imaging", "Medical Image processing and Techniques", "Medical Image Diagnostic", "Medical Image Diseases Diagnostic", "Diseases Diagnosis", "Disease Diagnostic Process", "Disease Diagnostic Techniques". We searched about 3000 articles to meet our keywords. Out of 300 articles 95 articles are redundancy articles. The remaining 205 articles are considered for systematic review. After reviewing these articles with their names, we found a new set of keywords such as "Artificial Intelligence", "Machine Learning", "Deep Learning", "Neural Network", "Disease Classification", and "Hybrid Diagnostic System" and 100 articles were omitted. Of the remaining 105 articles, out of these articles, 68 articles were excluded after deep reviews of 37 articles. Depending upon omission measures on articles we found some articles used Deep Learning and Machine Learning techniques. So, to develop a hybrid technique with good quality of diagnosis ability we combine both techniques with some modifications in the developed algorithm or by improvement of a common method and its development procedure for further research. By using PRISMA 2020 (Preferred Reporting Items for Systematic Reviews and Meta-Analysis) techniques we selected the most relevant articles for our research work, which is represented in Fig. 17. By using PRISMA 2020, we selected articles not only by automatic filter but also by considering the combinations of keywords and those articles gave the answers of our research questions, which are being discussed in Section 3.3.

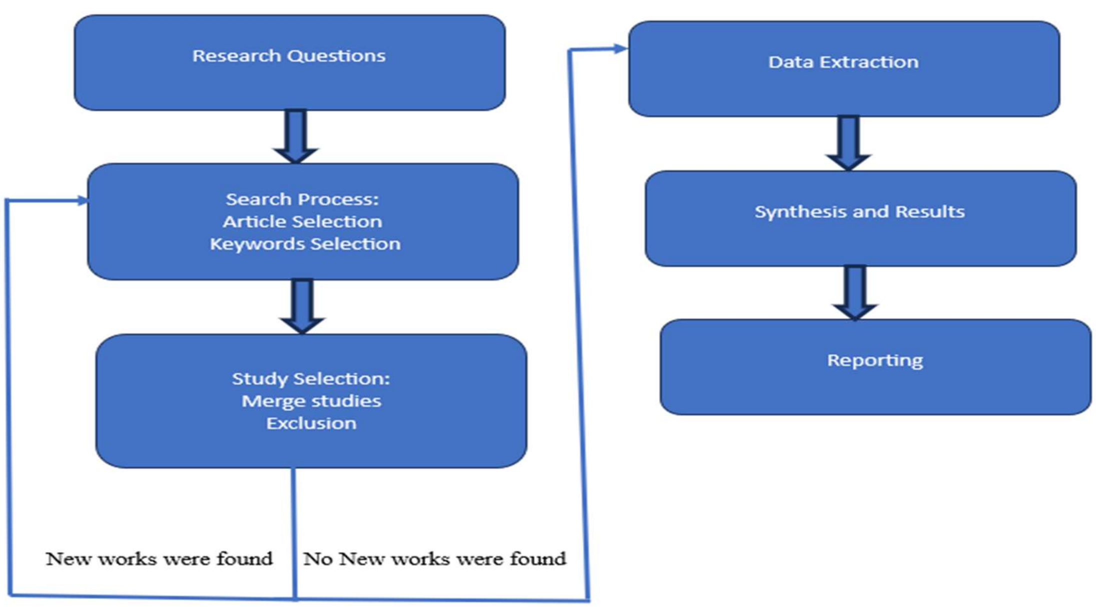

Figure 16: Literature Review Protocol

ISSN: 1992-8645 www.jatit.org E-ISSN: 1817-3195

Flow Diagram of Article Selection Procedure:

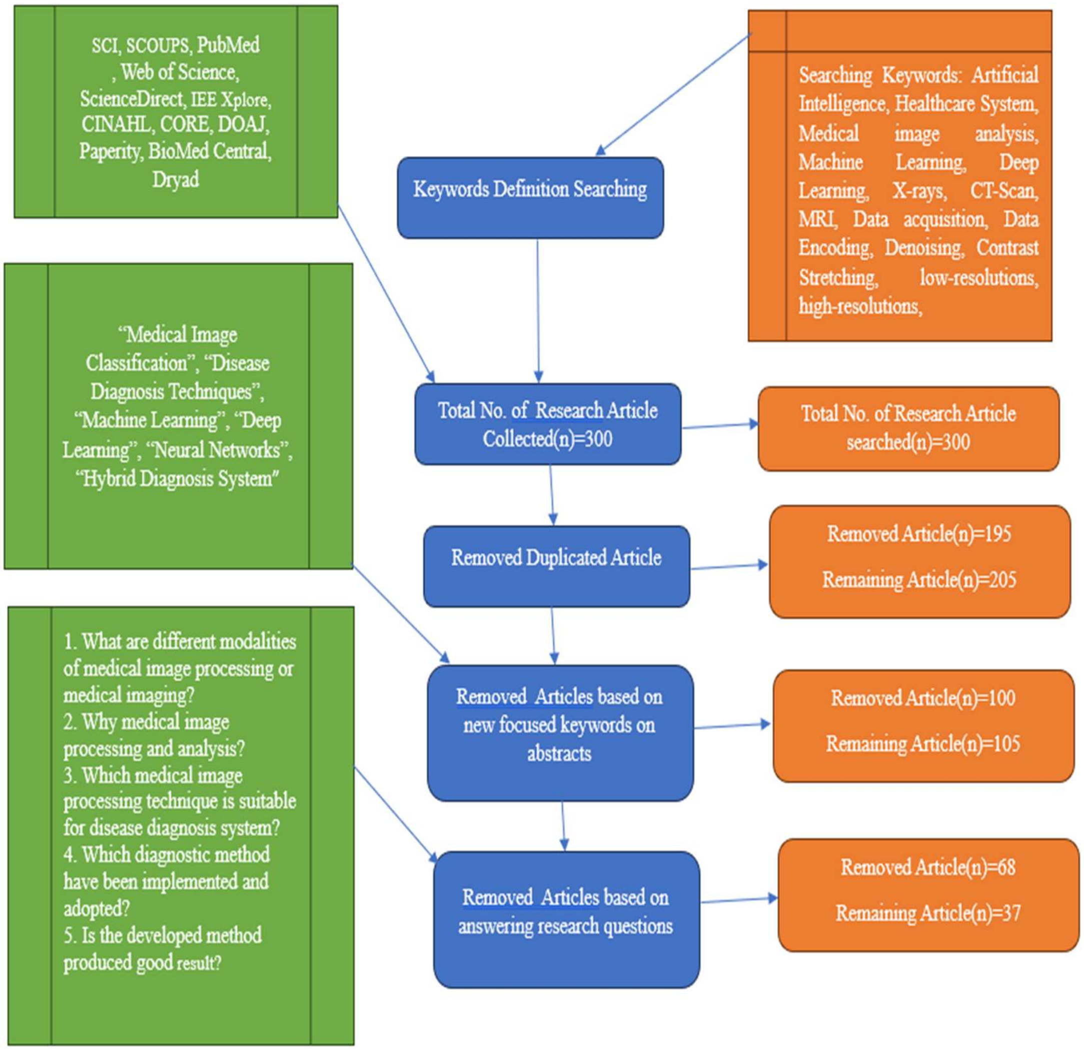

Figure. 17: PRISMA-2020 Representation of Article Selection Procedure

3.4 PRISMA 2020 Technique Output

After the inclusion and exclusion of research articles, the most relevant ones satisfied the research aims, which mostly explored the different concepts and techniques of medical image processing and disease diagnosis. We carefully review the included articles, extract, analyze, and compare the results to identify the most useful technique for feature research [33].

4. RESULTS OF SYSTEMATIC REVIEW

Here, we covered the theoretical underpinnings and practical uses of various medical imaging modalities in the first section. The second section covered medical image analysis using various imaging modalities [70].

4.1 Modalities of Medical Imaging System

Different modalities of medical imaging systems generate medical images. Medical images are crucial for healthcare professionals in diagnosing diseases and treating patients [34]. A group of digital image processing techniques called medical image processing can be used to get data from different medical image processing modalities that can be used to diagnose diseases and treat patients. These modalities may include magnetic resonance, ionizing radiation, optical methods, nuclear medicine, ultrasound radiations, etc., functioning as one-on-one modular media for disease diagnosis and patient treatment. Each modular media has particular features and responses to the structure of the human body [35]. It generates modalities that facilitate the capture of images of the internal structure of the human body or image samples, a feat not achievable with human naked-eye visibility [36]. There are several medical image modalities; out of them, some important modalities are addressed in our survey studies, which are exemplified in the following diagrammatic classification [63]

Table 1: Tabular representation of PRISMA 2020

Sr. No.	Article Collection Source Name	No. of Articles Collected	No. of Article Rejected	Reason for Rejection	No. of articles selected for Review
1	SCI	20	18	Keywords not matched	2
2	SCOPUS	40	35	Keywords and research questions not matched	5
3	PubMed	50	44	Keywords and research questions not matched	6
4	Web of Science	10	8	No. of pages <4 and not available relevant keywords	2
5	ScienceDirect	10	8	Keywords not matched	2
6	IEEE Xplore	30	28	No. of pages<4 and redundancy articles	2
7	CINAHL	5	3	Keywords not matched	5
8	CORE	2	1	Research questions not hold	1
9	DOAJ	56	55	Redundancy articles and not available relevant keywords	1
10	Paperity	7	6	Not relevant keywords	1
11	BioMed Central	65	56	Redundancy articles and not available relevant keywords	9
12	Dryad	5	4	Keywords and research questions not matched	1
Total		**300**	**266**		**37**

Graphical Representation of PRISMA-2020

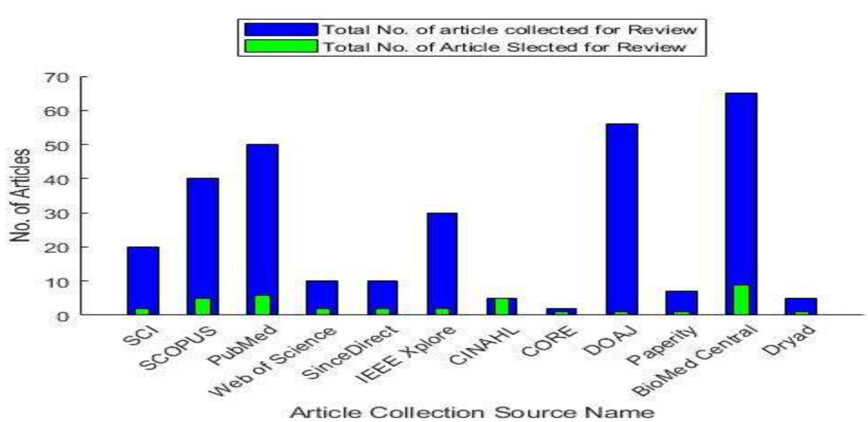

Figure 18: Bar chart representation of Article Selection Sources.

ISSN: 1992-8645 www.jatit.org E-ISSN: 1817-3195

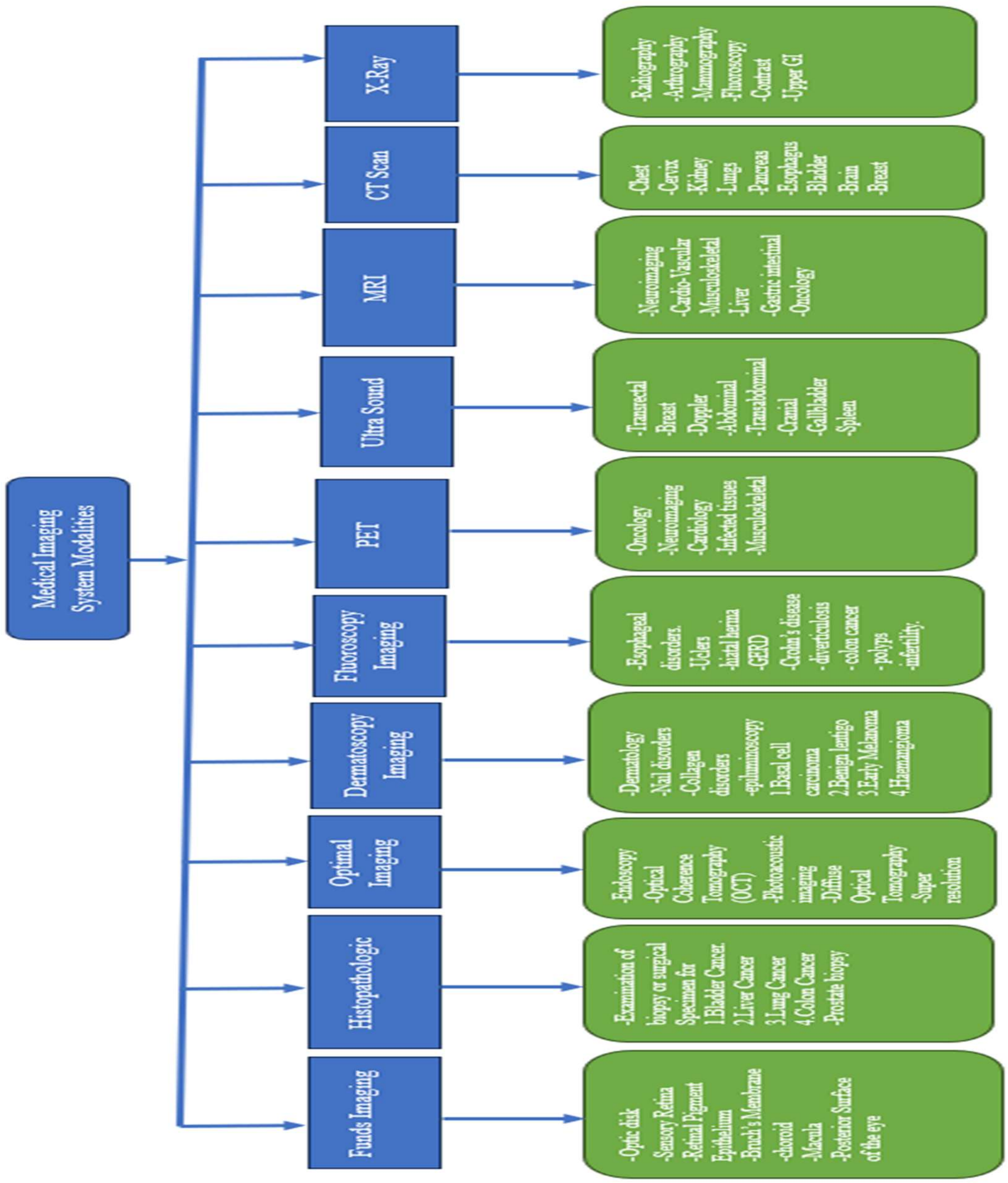

. Figure 19: Categorisation of Medical Imaging System Modalities

There are 4 imaging system modalities available in medical image acquisitions, such as 1. X-ray projection radiography and X-ray computed tomography imaging, 2. magnetic resonance imaging, 3. ultrasound imaging system, and 4. radio-nuclide imaging [37].

4.1.1 Physics of X-ray projection radiography and X-ray CT imaging

X-rays are electromagnetic waves and occupy the high-frequency range of the Electromagnetic (EM) Spectrum. X-rays are generated in a vacuum tube which consists of a 'Cathode' and an 'Anode'.

ISSN: 1992-8645 www.jatit.org E-ISSN: 1817-3195

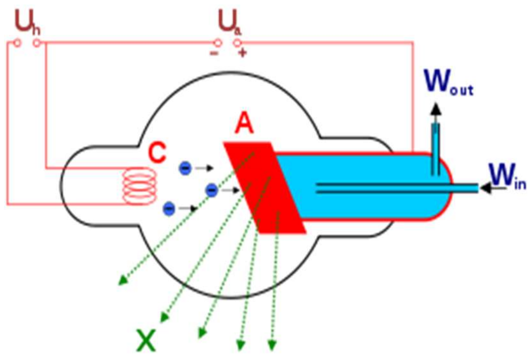

Figure 20: X-ray Imaging System [https://en.wikipedia.org/wiki/X-ray_tube].

X-ray Detectors are:

- ✓ **Screen/Film:** Directly exposed photographic film but is very inefficient. Typically, have an intensifying screen on both sides of the film. These screens are luminescent and emit light when exposed to X-ray.
- ✓ **Image Intensifier:** Used in fluoroscopy for low-dose real-time projection radiography, i.e., *Input Phosphor → Light →Photocathode → electron → acceleration by dynodes →Output phosphor → Light.*
- ✓ **Storage Phosphors:** Computed Radiography systems store the exposed image in photostimulable phosphors (PSPs). A laser scanner is used to stimulate the phosphor which emits light. Leads to a digitized image.
- ✓ **Flat Panel Detectors:** Digital Radiography using CCD, TFT, and CMOS based.

X-ray Computed Tomography imaging system produces a cross-sectional representation of the X-ray attenuation properties of the body. The patient body will be kept in front of the X-ray tube and the X-ray detector will produce cross cross-sectional image, i.e., *X-rays from tube → Patient → X-ray detector.* Using thin X-ray beamlines, projections are measured for the entire field of view. This is repeated for a lot of measurement angles of view. There are two types of Computed Tomography, such as axial tomography and linear tomography [38].

X-ray CT detectors are

- ✓ Scintillator Crystal with a photodiode.
- ✓ The scintillator converts X-rays into visible light, and the photodiode receives the visible light to produce an electric current.
- ✓ Scintillators are designed to have high absorption and transference to the photodiode.
- ✓ The digital data acquisition system connected to the photodiode converts the electric charges/current into a voltage signal and performs an analog to digital-conversion as well.

Another modern detector, in addition to the existing one, is currently under development. A photon-counting detector, a recent technological advancement, is about to make its debut. As described, it uses energy to improve image contrast:

- ✓ Photon counting detectors are direct conversion materials like CdTe or CdZne.
- ✓ It converts X-rays into an electric charge proportional to the X-ray energy.
- ✓ The signal produced is much higher, i.e., charge packets produced are much higher than in direct conversion.
- ✓ However, since the photons are binned according to energy there will be a proportional decline in photon statistics.
- ✓ Thresholds can be set to detect photons at different energies-enables counting.

X-ray CT data Acquisition

To capture the disease-affected body part of the patient, the patient lies on the bed along the Z-axis. The XY plane represents the cross-section of the patient, i.e., the linear attenuation coefficient of tissue. Parallel beam, fan beam, and cone beam are the different scanning configurations. In this figure 'D' is the bank of detectors, 'X' is a bank of X-rays, and 'T' is the X-ray tube are the parts of the Scanner. The images are reconstructed using typically back projection, iterative techniques, or more recently deep learning methods. The CT image intensity is referred to as Hounsfield Units (HU) [39, 41].

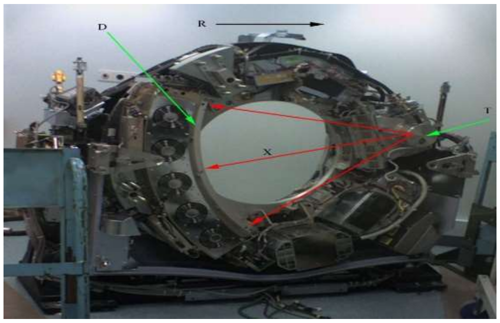

Figure 21: Computed Tomography Scanner [https://en.wikipedia.org/wiki/Operation_of_computed_tomography].

In X-ray Radiography, Image generation involves the following interaction [40],

I. **Compton scattering**: It has a deleterious or bad impact on the image quality-scattering of incident electromagnetic radiation, i.e., X-ray by the outermost electrons of the atoms. Depends on Electronic density, i.e., the atomic number and varies slowly with X-ray energy.

II. **Photoelectric absorption:** It has a positive impact on image quality-preferential absorption of incident radiation at k-edge energies leading to the ejection of electrons which are subsequently absorbed. Depends strongly on atomic number and diminishes with an increase in photon energy.

III. Rayleigh Scattering and Pair production do not contribute to image formation significantly in the diagnostic X-ray energy range.

4.1.2. Physics of magnetic resonance imaging

The following diagram shows the block diagram and Hardware Configuration of the Magnetic Resonance Imaging (MRI) Scanner. The MRI Scanner configuration is a combination of some hardware instrumentations of Magnet, Coils: Gradient-coils, RF coils, Electronics for receiving and transmitting, and Imaging Console, which are diagrammatically represented as follows [42, 43].

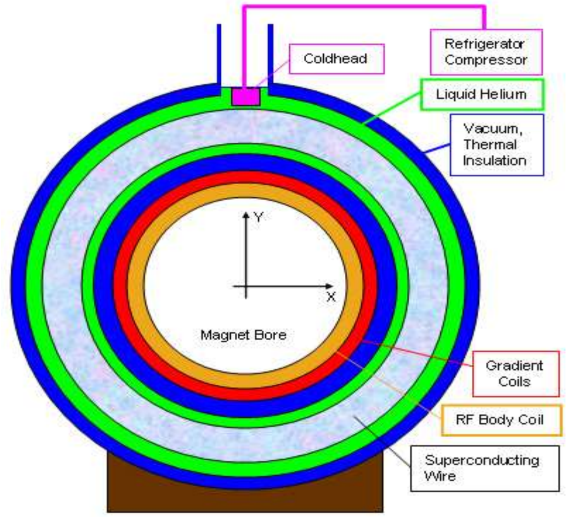

Figure 22: Super Conduct Magnet Design [https://mriquestions.com/superconductive-design.html].

Fig. 21 and Fig. 22 describe some superficial descriptions of MRI scanners. A magnet looks like a cylindrical Super Conducting Magnet. Niobium-Titanium wire immersed in liquid helium held at 4 Kelvin, superconducting at 9 kelvins. Helium is inside a cryostat, encompassed by liquid nitrogen and vacuum. Field strength can vary from 0.5 Tesla to 3.0 Tesla with research systems operating at 9 Tesla. Very high current is on all the time after energizing once at installation. Active and passive shimming and active and passive shielding are done [44].

Inside of the magnet bore gradient coils are fitted. There are 3-gradient coils. All are orthogonal to each other in the directions of physical axes X, Y and Z directions. At any cost orthogonal gradient coils never change their direction in magnetic field, they add an X, Y, and Z dependence on the magnetic field strength with the static field direction being along the Z-direction. X and Y dependency are produced by saddle coils and Z-gradient is done using two opposing coils wound around the circumference of the cylindrical bore [45].

Gradient Amplitude is limited by the current in the coils 100-200 Amperes which is a very high current. So, the maximum gradient amplitude is 1-6 Gauss/cm or 10-60mT/m. Switching times are of the order of 0.1 to 1ms. But the slew rate is the maximum rate of change of the gradient value mT/m/ms. Eddy currents can be induced in the metallic components of the magnet housing- distorting the gradient fields [47].

There are some limitations due to Gradient coils. Such as, Self-inductance of the gradient coil prevents rapid switching of the gradients. Coils can be made smaller, leading to reduced Field of view. Eddy currents can be induced in patients causing peripheral nerve stimulation. The limit is 40T/s beyond which the risk of peripheral nerve stimulation is not negligible [46].

Radio Frequency (RF) Coils induce the spin precession as well as measure the currents induced by the spins. Volume coils and surface coils are also used. Volume coils surround the patient and Surface coils are placed nearby of the patient's surface or on it. Arrays of surface coils are used to improve sensitivity [49]. The body coil is referred to as a birdcage resonator. Head coil-birdcage, saddle coil, or Alderman-Grant coil designed to fit the human head. Specialty volume coils like knee, neck, and small extremity coils are also available. Body coils are just inside gradient coil is used to transmit and another coil near the volume of interest is used to receive the signal transmission and reception require very different current amplitudes in the coil [46].

There is typically a scanning console called a diagnostic device. The console interfaced with the MR hardware is used to select imaging planes, and set ECG gating, and respiratory gating. The data acquired is passed to a reconstruction engine-array processor which reconstructs about 10-50 images per second [47].

MRI data acquisition

1. Slice selection gradient

Given a fixed B_0 field, the Larmor Precession Frequency is the same throughout the sample. The signal obtained from the induced EMP cannot be localized, i.e., X, Y, and Z positions cannot be estimated. The first step is to isolate the cross-section by applying gradient fields. We know the Gradient along the Z-axis. So, let's consider the application of a slice selection gradient (0, 0, G) yields a Larmor frequency that is a function of Z, i.e., $V(Z) = \gamma(B_0 + G_z \times Z)$. Application of RF excitation at a specific frequency would excite a thin section of the sample. The section or slice would correspond to all points whose Z position has the specific field-dependent Larmor frequency. Given a position-dependent magnetic field strength, we can now excite the spins in a 'slab' of the sample using an appropriate RF pulse. For the same RF frequency range, we will gate thicker or thinner slabs based on the strength of the gradient. A strong gradient will lead to the selection of a thicker slice for the same range of RF frequencies [48]. So Mathematical model of the RF waveform of the signal is $S(\gamma) = Amplitude(A) \times rect(\gamma - \gamma')/\Delta\gamma$.

2. Frequency encoding

The signal received is the integration or summation of signals from the excited slice. No x, y information is present in the signal. Spatially encoding MR signals within the image plane is called Frequency encoding. The gradient is turned on during FID. The direction of the frequency encoding gradient is called the readout direction. The readout direction is orthogonal to the slice selection gradient. Typically, the readout direction is the X-axis with the Z-axis along the length of the sample, i.e., patient.

3. Phase encoding

If frequency encoding is used for readout along the 'u' direction then phase encoding is for readout along the 'v' direction. Slice selective RF pulse is applied followed by a refocusing gradient. The y-gradient pulse with strength G_y is applied and duration T_p achieves phase encoding. A readout direction gradient is applied while acquiring data. The pulse sequence is repeated to cover the entire k-space trajectory.

4. Image reconstruction

Data acquired from 2D MR imaging pulse sequences can be interpreted as scans of Fourier Space. Taking the inverse Fourier transform of the signal will yield the image. Fourier space is sampled, so a 2D Discrete Fourier Transform algorithm is required for reconstruction. Interpretation of images is not straightforward as the meaning of the quantity being reconstructed cannot be explained like in CT or radionuclide imaging. Contrast in images depends on the imaging parameters, like the time to echo and pulse repetition time [50].

ISSN: 1992-8645 www.jatit.org E-ISSN: 1817-3195

4.1.3: Physics of Ultra Sound (US) Imaging

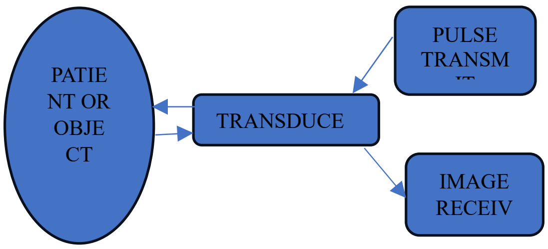

Figure 23: Basic Ultrasound System.

A basic Ultrasound system consists of a piezoelectric transducer and associated circuitry. The transducer is the most important part of the system. A transducer consisting of the piezoelectric crystal with an electrical signal lead to a mechanical pulse that travels through tissue. The longitudinal pulses reflect off mechanical inhomogeneities, i.e., boundaries between different acoustic properties. The echo time is 2z/c. Here speed 'c' is 1500 m/s. The reflected signal indicates a boundary at depth tc/2. The lateral extent varies with depth, i.e. the ultrasound beam spreads out as depth increases. Since the transducer is a piezoelectric crystal, that crystal produces US waves when an electric field is applied. The electric field causes strain that leads to a US wave [51]. They induce electric potential due to strain or mechanical displacement. Lead Zirconate titans or PZT is the piezoelectric crystal characterized by transmitting constant 'd' and receiving constant 'g'. The electric signal is usually an impulse applied for a short duration of time leading to the production of US waves. The propagation of US waves results in compression and relaxation of small volumes of tissue which results in pressure change at that location. Propagation of the US can be described in terms of a spatially and temporally varying pressure function. Traditionally, it is described in terms of displacement and velocity of the particles in the medium of propagation.

The transducer transmits and receives ultrasound energy. In ultrasound imaging, the ultrasonic waves are reflected and scattered by anatomic structures. The reflected and scattered waves are measured to obtain the image. The reflection and scattering vary between tissues providing contrast [61]. There is no reconstruction but rather localization of ultrasound to a limited volume. 2D imaging is done by focusing and steering the US beam. US frequency range is above 20KHZ, right above the threshold of human hearing. Medical US is between 1-10 MHZ. US propagation is the sound propagation [52]. The most common applications are as follows

- ✓ Echocardiography: This imaging system generally uses sound waves to create a live picture of the heart. It shows blood flows in the heart and heart valves. Doppler imaging helps to measure velocities, for instance, blood flow. Because of its non-ionizing and non-invasive nature, this imaging system is widely used in Obstetrics.
- ✓ Fetal Ultrasound or Utero Imaging: This US imaging system is generally used to check a baby's heart during pregnancy. It provides real-time heart imaging of an unborn baby without surgery or X-rays.
- ✓ Real-time imaging systems can be used in image-guided surgery.

There are different modes of scanning ultrasound mechanical scanners. An A-mode scan is done by recording the echoes or reflected pulses as a function of time along the Z-direction. 2D and 3D mode scans are obtained by moving the 'beam' in X and Y directions [60]. This can be done mechanically or electronically "steered". By putting together all the line scans in the form of a Grayscale matrix one can get the B-scan or image. Image pixel values indicated reflectivity in the body denoted by R (x, y, z). Surface reflections are from the interface of 2 materials determined by acoustic impedance $Z = \rho c$, where ρ is the density of material in (kg/m^3) and c is the velocity of acoustic waves(m/s). Acoustic Ohm's law $Z=\frac{P}{V}$, where P is the pressure (1Pa=N/m^2= =kg/ms^2) and V is the particle velocity. Here particle refers to the microscopic particles of the medium i.e., tissue in medical US [53].

The reflectivity from an interface can be defined as $R=\frac{Z_2-Z_1}{2\times Z_0}$ where z_2, z_1, and z_0 are impedance and the average impedance $Z_0 = \frac{Z_2+Z_1}{2}$. Reflections provide only a small signal i.e. the SNR is low.

4.1.4 Physics of radionuclide imaging

Nuclear medicine is referred to as Nuclide imaging. In this imaging system, a radioactive substance like γ-rays is introduced into the body. Time is allowed for the distribution and metabolism or uptake of the radioactive compound. This is called functional imaging [55]. Variation in concentration of the compound depends on the presence or absence of physiologic function.

In nuclear medicine, a tracer molecule is administered to the patient usually by intravenous injection. A tracer is a molecule carrying an unstable isotope radionuclide. These isotopes emit gamma radiation, i.e., high energy photons while at the same being metabolized by the human body. The gamma radiation emitted is proportional to the concentration of the tracer, as the tracer is a function of position and time. This means that we can do functional imaging with radionuclide imaging [57].

Radioactive decay is the rearrangement of nuclei to lower energy states which corresponds to a greater mass defect. The parent atom decays to a daughter atom which has higher binding energy/nucleon. A radioactive atom is said to decay when its nucleus is rearranged. A disintegration is a radioactive atom undergoing radioactive decay, accompanied by the release of energy [62].

A proton is transformed into a neutron and a positron (anti-electron). The mass number A does not change, the proton number or atomic number Z reduces. Positron combines with electrons and annihilates resulting in the release of two 511 keV photons that are used for medical imaging, Positron Emission Tomography. For example, Fluorine-$F_9^{18} \rightarrow O_8^{18} \rightarrow V_e + e^+ \rightarrow$ Beta plus decay [56].

A radionuclide loses energy by emitting gamma rays and in the context of diagnostic imaging, is of range from 60 keV to 600 keV, which is the same as range of X-rays. For example, $Dy_{66}^{152} \rightarrow Dy_{66}^{152}$ + gamma rays. This is called gamma photon, which is used in Single Photon Emission Computer Tomography (SPECT). Positron-emitting tomography (PET) is another modality of radionuclide imaging system. The emitted positron travels several mm in tissue before it combines with an electron and emits two gamma photons (511 keV). These two gamma photons travel opposite from the point of emission with two anger cameras 180 degrees apart. Both these photons can be recorded simultaneously. A set of detections in the two cameras are considered true detection if they fall within a time window (2-20 ns). This is called annihilation coincidence detection (ACD). Coincidence detection means that the annihilation event occurred along the line joining the two detecting pixels. The heads are rotated to collect the data at different angles for tomographic reconstruction [54].

Data acquisition

Detection is accomplished by photomultiplier tubes/photodiodes coupled to a scintillator-anger camera or gamma camera. Scintillator crystal absorbs high energy gamma rays by photoelectric absorption. The electrons resulting from photoelectric emission travel through the crystal interacting with multiple electrons and releasing the energy in the form of light photons. A large crystal connected to multiple PMTs measures the signal [58, 59].

5. PERFORMANCE COMPARISON OF EXISTING DIFFERENT NETWORK MODELS

Pictures with PSNR values between 40 and 45 dB are easier for the human eye to perceive. Table 2 presents the performances of various neural network models. The table displays the performance in terms of PSNR values in dB for the output results of various network models. Primary sources provide all the data. The two most common data sets used as benchmarks for high-resolution natural images are set1 [64] and set2 [65]. To compare the PSNR values of various results from different existing models, we are only using 4 of the 15 images in Dataset 2, while Dataset 1 contains 4 images. Below, you will find the dataset figures.

Figure 24: Row-1 contains images of Datset1and Row-2 contains images of Dataset2[64, 65].

Table 2: PSNR value comparisons of existing different models

Sr. No.	Existing Model Name	Average PSNR Value of Dataset1	Average PSNR Value of Dataset2
1	SRCNN [2]	30.49	27.61
2	VDSN [9]	31.35	28.03
3	DRCN [10]	31.53	38.04
4	DRRN(B1U25) [11]	31.68	28.21
5	ESPCN[12]	30.9	27.73
6	FSRCN[13]	30.55	27.5
7	EDSR[43]	32.46	28.8
8	EDSR+[43]	32.62	28.94
9	LapSRN[41]	31.33	28.06
10	SRGAN[24]	29.4	26.02
11	SRDenseNet[60]	32.02	28.5
12	RDN[42]	32.47	28.81
13	RDN+[42]	32.61	28.92

The results of various deep learning models using neural networks are displayed in the table above. Each image receives a PSNR value as input, and we express the output as a numerical value. By averaging the PSNR values of all processed images, we can determine how well a given model performs. We calculated the PSNR values using a scaling factor of 4, and all models exhausted it. Adding a plus sign to a model's name indicates that it has self-accumulation capabilities [64, 65].

Graphical Representation of Reviewed Model PSNR values:

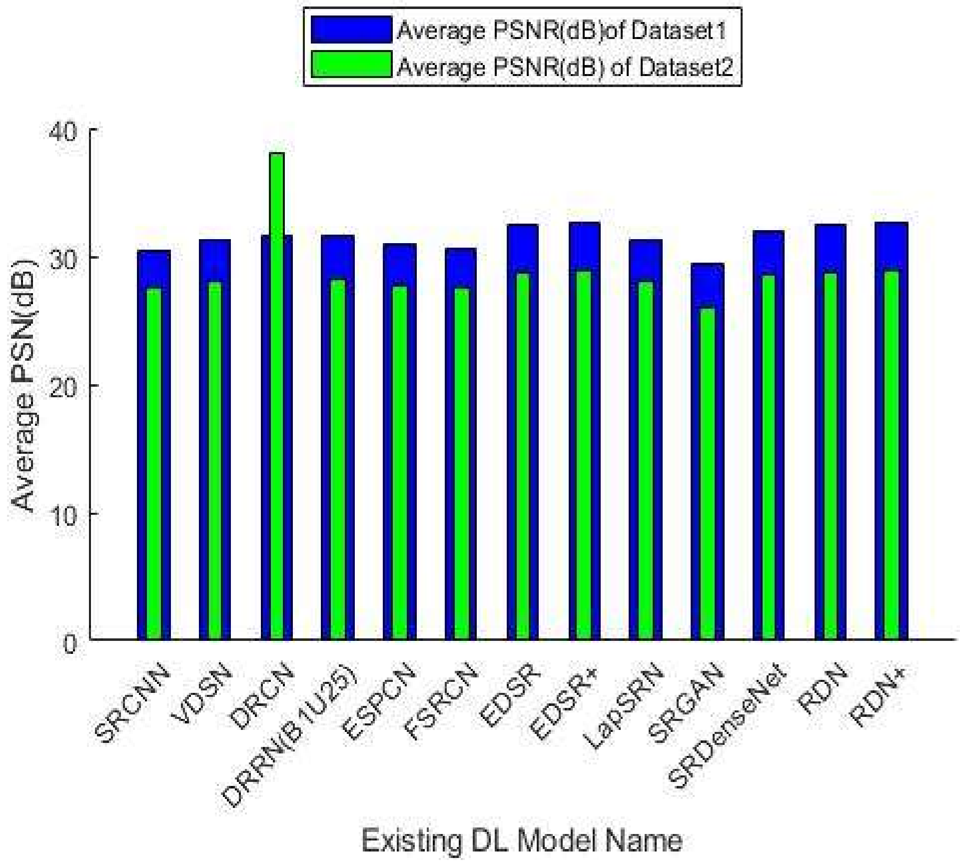

Figure 25: PSNR values Comparisons among different Existing Models using Bar Chart.

6. DISCUSSION

Deep learning applications play a crucial role in medical image processing, advancing research and development for various tasks such as image classification, edge detection, and segmentation [66, 67]. Deep learning is nothing but that cascade of nonlinear transformations. It is essentially a process of learning from beginning to end. Generally, this learning is called deep learning because we want to extract more and more information from the input data. This information may be low-level information, mid-level information, or high-level information. We can represent deep learning as a cascade of nonlinear transformations.

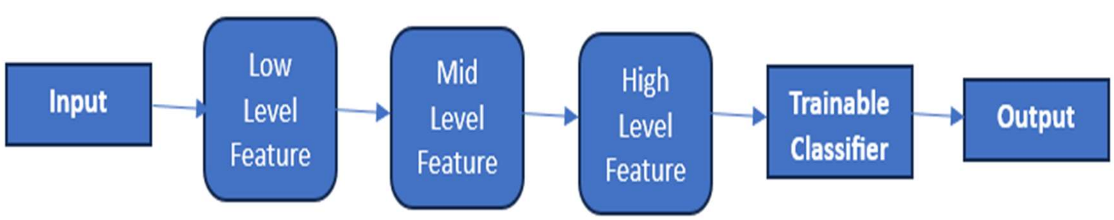

Figure 26: Hierarchical Representation of Deep Learning Model.

ISSN: 1992-8645 www.jatit.org E-ISSN: 1817-3195

When working with images as an input, we can classify their pixel values and edges as low-level features; texture and motif are examples of mid-level features; and object parts and objects themselves are examples of high-level features, i.e.,

$Pixel \rightarrow Edge \rightarrow Texture \rightarrow Motif \rightarrow Part \rightarrow Object.$

So, if the input is text, we can classify words and characters as low-level information, word groups and clauses as mid-level features, and sentences and stories as high-level information in the context of text recognition., i.e.,

$Character \rightarrow Word \rightarrow Word - Group \rightarrow Clause \rightarrow Sentences \rightarrow Story.$

So, in hierarchical representation, each deep learning module mimics the brain's cortex by elevating its input representation to a higher level.

Deep learning techniques are finding more and more applications in medical imaging, particularly in the realm of high-resolution image reconstruction. After coming up with potential uses, medical image analysis researchers create an architecture that allows for improved performance boosts and offers a user-friendly model for analysis and research [68].

There are two major obstacles in the area of medical image analysis. The first is that there aren't any restrictions on specific images, and the second is that there aren't any high-quality references. As a result, obtaining high-resolution ground truth images for clinical imaging is a challenging task. In this brief summary, we have covered various methods to vaccinate specific priors and some limitations on data augmentation [69].

We have utilized 1D Wavelet Transform [86] for high-resolution image restoration or reformation, except for the machine learning technique. We would like to know what sets our study apart from others that have been published.

6.1 Answers to Research Questions

After a rigorous review of inclusion articles information was extracted and found that they can explain and clarify the answers to research questions.

"Q1: In medical imaging and image processing, what are the various modalities? Section 3 of this article acknowledges the various medical image analysis methods and procedures for identifying and diagnosing diseases. Many medical conditions, including those affecting the lungs, heart, brain, and cardiovascular systems, can be better diagnosed with the use of magnetic resonance imaging (MRI). Many medical conditions, including those affecting the bones, lungs, and liver, can be better diagnosed with the use of CT scans. Imaging techniques used in the US, like echocardiography, fetal ultrasound, ureter imaging, and image-guided surgery (which uses real-time imaging systems), can be used to diagnose several diseases. A number of diseases, including pneumonia, breast cancer, and osteoarthritis, are being diagnosed using the X-ray imaging modality. Several skin diseases and Alzheimer's disease are now being diagnosed using the PET imaging modality [70].

"Q2: Why medical image processing and analysis?" According to the systematic review of included articles, the main goal of medical image processing and analysis is to help patients find diseases early and get better by processing and analyzing medical images of different parts of the body.

"Q3: Which medical image processing technique is suitable for high-resolution image reconstruction and disease diagnostic system?" We found that filtering techniques work better for precise edge or border ROI recognition throughout the inclusion article analysis. To eliminate noise, one can use a median or low-pass filter; to maintain the borders of the ROI, one can use edge detection and contrast enhancement techniques. Additionally, histogram equalization and matching can be employed for color normalization, which enhances contrast. Additionally, it was noted that different types of transforms were utilized to extract significant features. It is possible to find conditions in domains other than space using tools like Wavelet and Fourier transform. Image segmentation is a critical step in the disease diagnostic process, particularly when working with medical images due to the increased information content and the fact that the borders or edges of ROI contain important details for accurate disease identification and diagnosis. Whether you're working with a single image, a set of images, or more complex (Otsu) image criteria, the gray-level segmentation technique is the simplest and most effective method. Active contour detection and modifications, such as Snake, are used in the majority of human illness diagnostic processes. The segmentation process has made use of a number of different clustering techniques. In order to segment the ROI K-mean, for instance, fuzzy C-means are employed.

"Q4: Which High-resolution image reconstruction method has been implemented and adopted?" We saw that many neural network models, like SRCNN, VDSN, DRCN, ESPCN, EDSR, FSRCNN, LapSRN, SRGAN, SRDensenet, RDN, and many more, have been used to reconstruct high-resolution images from low-resolution images. These models of generative adversarial networks (GANs) and convolutional neural networks (CNNs) can release PSNR values on specific constraints that are visible to the human eye. In an effort to improve human visualization, we set out to build a new high-resolution model.

"Q5: Has the developed method produced good results?" In the reference methods, the high-resolution images were produced by the system that was already developed in the inclusion articles, with average PSNR values ranging from 27 dB to 38 dB. The PSNR values of medical images, however, range from 35 dB to 45 dB, which allows for better human visualization. That being said, our developed algorithm, Algebraic Mean Compression (AMC), is a modified compression technique. It demonstrates superior performance in the enhancement of high-resolution images relative to current CNN models. It has achieved 90% accuracy, pertaining to PSNR, MSE, and SSIM.

6.2 Data Scarcity

During the time of data paucity, there is a need for data augmentation for an increasing number of datasets. Generally, data augmentation comprises scaling, translation, rotation, flipping, changing brightness, adding noises, contrasting images, modifying colors, gamma-transformations, and many more.

Except above operations, researchers are using deep learning techniques for data augmentation to increase the dataset. The transfer learning of *Zhang et al*. [71] is used to increase the dataset also. His proposed method SIFT (Scale Invariant Feature Transform) is used to extract features over available medical images match the extracted features with available features of medical images and add the matching sub-regions to avoid dataset scarcity.

The "Smart augmentation" model of *Lamely et al*. [72] also helps to fulfil the data scarcity of the data set by employing a network. The network will generate another new image based on matching features of at least two images of the training dataset. We know images are classified based on different parameters and several networks have been trained such that they have synthesized differently to form a new image. So, *Shin et al.* put headfirst the use of GAN to synthesize medical images in the segmentation process [73].

Cubuk et al. proposed a method, that will perform data augment automatically [74]. In the proposed method they used 5 sub-polices. To predict 5 sub-polices they used a controller. The controller is nothing but a recurrent neural network and the sub-polices are achieving data augmentation by performing either translation or rotation operation. Every neuron activity consists of a set of sub-activities that are pigeonholed by two parameters such as probability and magnitude. Probability has a role in applying sub-polices and magnitude has a role in using the sub-polices. And the controller is trained in such that, it will choose sub-polices for a particular database based upon reward signals. The sub-model has been trained with data augmentation through the carefully chosen sub-police. Readers are advised to see detailed implementations [74, 75].

Data augmentation is a special tool, specifically suitable for small datasets. It is notable that in the case of medical imaging and its application, the data augmentation should be strictly consistent because, in the case of tumor analysis, the color of tissue has a vital role in distinguishing between disease-affected tissue and disease-free tissue, but due to data augmentation the color may degrade the performances of test approach.

6.3 Adding Prior

In the cases of medical images dataset, natural images dataset, and IHS images dataset need priors to improve the performances of high-resolution techniques. *Liang et al.* introduced a feature extraction layer before the integration of gradient, by keeping the parameters fixed [76]. In the meantime, outstanding investigations done in [67], can also be observed as handcrafted prior information. Although we know that there is a drawback of this prior, there is the use of hyper-parameters which is vital but need to be chosen empirically for each dataset sample.

The denoising network method of *Lehtinen et al.* [77] is trained with only the denoising of noisy images, i.e., no images of the dataset are clean images. So, in the training process, both input images and output images are noisy, i.e., output noisy images are clean images with different noise ratios. A noisy image is sufficient for denoising tasks, during the time of processing stage. But one important thing is that the author has assumed here, that the average value of noise is zero. In this point of view, the author has explained here that, if the average noise is zero, then the average of a set of noisy images is a noise-free or denoised image. However, the demerit here is that since the network has been trained with stochastic gradient descent methods, it leads to an inaccurate optimization direction. So, the author has taken the average gradient point for the correct optimization direction.

7. FUTURE CHALLENGES IN HIGH-RESOLUTION IMAGE RECONSTRUCTION

In the aforementioned sections, we reviewed existing methods of super-resolution or high-resolution image reconstruction, which have been frequently used. In this section, we exemplify some future challenges or advanced technical issues that are treated as crucial open challenge problems in the area of super-resolution or high resolution.

7.1 High Resolution Given Registration Error

Registration is one of the most important steps to perform the image reconstruction successfully. Therefore, there is a need for a correct registration scheme based upon a robust motion model of multiple object motion, transparency occlusion, etc. [78].

However, we are not ensuring the correctness of the registration algorithm of the SR image reconstruction method, we shall not certify the performance of the registration algorithm in certain domains. So, an error that occurred due to inappropriate registration would be considered during the reconstruction process. Although most of the super-resolution reconstruction algorithms implicitly considered registration error as white Gaussian noise, still most sophisticated models need this error for their performance analysis.

Bose *et al.* [79] proposed the total least square method to minimize the error generated by inaccurate registration. In this method they have shown the error generated due to inaccurate registration is represented as system matrix W_k. And this will help to improve solution accuracy when an error occurs not only during the recording process but also in the measurement matrix.

Lim *et al.* [80] approached the adoptive regularization method to minimize the effect of errors that occurred due to inaccurate registration. The basic idea of this method is that the low-resolution (LR) image having more registration error should be less subsidized to the reconstruction of high-resolution images than the reliable low-resolution images. For this, they extended their work based on a set-theoretic approach. In this approach, they proposed a regularization function that works on data consistency terms. So, the minimization function is defined as

$$\sum_{k=1}^{p} \lambda_k (x) \ \parallel y_k - W_k x \parallel^2 + \parallel C_x \parallel^2 \quad (15)$$

Where,

$\lambda_k (x)$ = Is the regularization function

y_k = Is the Low-resolution image

W_k = Is the System Matrix

C_x = Is the Smoothness matrix or high pass filter

$\parallel .. \parallel^2$ = Is the L_2-norm

But subject to constraint

$$\lambda_k (x) \propto \frac{1}{\parallel y_k - W_k x \parallel^2}$$

$$\lambda_k (x) \propto \parallel C_x \parallel^2$$

$$\lambda_k (x) > 0$$

Note:
λ_k (x) considers the influence of the cross – channel

7.2 Given Blind High-resolution Image Reconstruction

In most algorithms of high-resolution image reconstruction, the blurring process is accepted to be known. Whereas in many practical situations, generally blurring processes are unknown or only known through the set of parameters. So, it is need to integrate the identification of blur during the reconstruction of high-resolution images.

In this problem, we may follow the procedures of Nguyen *et al.[81]* proposed parametric technique for blur identification and regularization process, which is based on generalized cross-validation (GCV) and Gaussian quadrature theory. For the minimization of these unknown blurring parameters, they used a solution of multivariate nonlinear minimization problem statement.

7.3 Identification of Computationally Competent SR Algorithms

To reduce the computational cost, it is very important to develop an efficient or competent SR algorithm, in such that it will be suitable for application in practical situations. However, there is indeed a need for a large computational load for the implementation of the inverse procedure in a super-resolution (SR) algorithm. As per earlier discussion, the interpolation-based approach and adaptive filtering approach are more suitable for real-time applications. But another issue is found in [82, 83] effort concerning.

Nguyen *et al.* [82] to solve the issues of the Tikhonov-regularized SR algorithm, introduced a technique "circulant block preconditioners" for the acceleration of the conjugate gradient (CG) method. This preconditioner technique helps to transform of original system into another system in such that rapid conversion will be possible without changing solutions. The main goal for the derivation of preconditioners is that since the convergence rate of conjugate gradient depends upon the distribution of eigenvalues of system matrix W_k, it makes the convergence rate slow. So, to make faster convergence of low-resolution channels they introduced a preconditioned system with eigenvalue clustering is done.

In developing the method of the SR algorithm, authors Elad and Hel-Or [83] have proposed the separation procedure of fusion and deblurring. To reduce computational complexity, they have assumed noises or blurs are space invariant and that will be the same for all experimental images. The geometric deviations among measured images are pure transformations, and the additive noise is white Gaussian noise. Even though this fusion SR algorithm is limited in assumption, still then it is still iterative and simple. But it preserves its optimality in the sense of machine learning.

8. CONCLUSIONS AND FUTURE WORK

This extensive review covered advancements in medical image analysis, various modalities of medical imaging acquisition and their respective applications, and state-of-the-art deep learning techniques for high-resolution natural images. In CT, deep learning is often used for image processing tasks like segmentation, edge detection, classification, Image compression and object detection. It can also be used to evaluate the stage of a disease and its treatment, remove noise and artifacts, and do other similar things. On the other hand, deep learning techniques are often used in Positron Emission Tomography (PET) imaging to do things like remove noise, sort images into groups, predict how well a treatment will work, and estimate newborn Tetralogy of Fallot (TOF).

Depending on the dimensionality of the images, deep learning schemes can be categorized based on whether they use 2D or 3D input readings for medical image data. When dealing with 2D natural image datasets, 2D convolutional neural network (CNN) deep learning typically proves to be the optimal choice. 2D convolutional neural networks (CNNs) might not be the best choice for analyzing certain medical images, such as 3D volumetric images from CT and PET scans. Compared to 2D CNN, 3D CNN DL methods require more data and are more complicated. Preservers for 3D convolutional neural networks allow for the preservation of both local and global spatial data.
Researchers in the fields of biomedicine and medical imaging may find this survey encouraging for their future work. We anticipate the DL technique to become standard technology in the field of medical imaging systems in the near future. Therefore, we anticipate the imminent development of the NEW DL method: 1. “Compression Engine: A Compression Software” and 2. “A Modified Framework for Reversible Digital Image Watermarking” which are enable the recovery of high-resolution images from low-resolution ones. In this regard, we have started work on image compression and image watermarking techniques [03, 28]. Future research may develop medical image analysis techniques for security purposes [85].

ISSN: 1992-8645 www.jatit.org E-ISSN: 1817-3195

CONFLICTS OF INTEREST

The authors declare that they have no conflict of interest.

ACKNOWLEDGMENT

This work has been supported by the SERB, Govt. of India: [Grant Number SUR/2022/004482].

REFERENCE:

[1] C. H. Pham, A. Ducournau, R. Fablet, and F. Rousseau, "Brain MRI super-resolution using deep 3D convolutional networks", *IEEE 14th International Symposium: Biomedical Imaging (ISBI 2017)*, April 2017, pp 197-200, DOI: 10.1109/ISBI.2017.7950500.

[2] C. Dong, C.C. Loy, K. He, and X. Tang, "Learning a Deep Convolutional Network for Image Super-Resolution" *In: D. Fleet, T. Pajdla, B. Schiele, T. Tuytelaars, (eds) Computer Vision – ECCV 2014. ECCV 2014. Lecture Notes in Computer Science*, vol 8692. Springer, Cham., September 2014, DOI:10.1007/978-3-319-10593-2_13

[3] P.K. Sahoo, D. Gountia, R.K. Dash, and J. Mohammed, "A Technical Analysis of Digital Image and Video Processing", *Taylor & Francis Journal on the IETE Technical Review (TITR),* 2023, pp 1-11, DOI: 10.1080/02564602.2023.2262418.

[4] D. Gountia, and S. Roy, "Security Model for Protecting Intellectual Property of State-of-the-Art Microfluidic Biochips" *Elsevier Journal of Information Security and Applications (JISA),* 2021, pp 1–15,DOI: 10.1016/j.jisa.2021.102773.

[5] K. H. Jin, M.T. McCann, E. Froustey, and M. Unser, Deep Convolutional Neural Network for Inverse Problems in Imaging. *IEEE Transactions on Image Processing*, 2017, Vol. 26 No. 9, pp 4509-4522. DOI: 10.1109/TIP.2017.2713099.

[6] Q. Yang et al., "CT Image Denoising Using a Generative Adversarial Network with Wasserstein Distance and Perceptual Loss", *IEEE Transactions on Medical Imaging, Low-Dose*, 2018. Vol. 37, No. 6, pp 1348-1357. DOI: 10.1109/TMI.2018.2827462.

[7] Ronneberger, Olaf, et al., "U-Net: Convolutional Networks for Biomedical Image Segmentation", December 2015, DOI: 10.48550/arXiv.1505.04597

[8] Geert Litjens, Thijs Kooi, Babak Ehteshami Bejnordi, Arnaud Setio, Francesco Ciompi, Mohsen Ghafoorian, Jeroen van der Laak, Bram Ginneken, and Clara Sánchez, "A Survey on Deep Learning in Medical Image Analysis", *Medical Image Analysis,* 2017, Vol. 42. DOI: 10.1016/j.media.2017.07.005.

[9] J. Kim, J.K. Lee, and K.M. Lee, "Accurate Image Super-Resolution Using Very Deep Convolutional Networks", *IEEE Conference on Computer Vision and Pattern Recognition (CVPR),* June 2016, pp 1646-1654. DOI: 10.1109/CVPR.2016.182.

[10] J. Kim, J.K. Lee, and K.M. Lee, "Deeply-Recursive Convolutional Network for Image Super-Resolution", *IEEE Conference on Computer Vision and Pattern Recognition (CVPR),* June 2016, pp 1637-1645. DOJ: 10.1109/CVPR.2016.181.

[11] Y. Tai, J. Yang and X. Liu, "Image Super-Resolution via Deep Recursive Residual Network", *IEEE Conference on Computer Vision and Pattern Recognition (CVPR),* July 2017, pp 2790-2798. DOI: 10.1109/CVPR.2017.298.

[12] W. Shi et al.. "Real-Time Single Image and Video Super-Resolution Using an Efficient Sub-Pixel Convolutional Neural Network", *IEEE Conference on Computer Vision and Pattern Recognition (CVPR),* June 2016, pp 1874-1883. DOI: 10.1109/CVPR.2016.207.

[13] W. Ruangsang, S. Aramvith, and T. Onoye, "Multi-FusNet of Cross Channel Network for Image Super-Resolution", *IEEE Access*, 2023, 11, pp 56287-56299. DOI: 10.1109/ACCESS.2023.3282571.

[14] Alex Krizhevsky, Ilya Sutskever, and Geoffrey Hinton, "ImageNet Classification with Deep Convolutional Neural Networks", *Neural Information Processing Systems*, 2012. DOI: 25. 10.1145/3065386.

[15] Z. Chen, Y. Wu, N. Zhang et al., "High temporal resolution total body dynamic PET imaging based on pixel-level time-activity curve correction", *IEEE Trans. Biomed. Eng.* 2022, pp 3689–3702. DOI: 10.1109/TBME.2022.3176097.

[16] M. T. McCann, K. H. Jin, and M. Unser, "Convolutional Neural Networks for Inverse Problems in Imaging: A Review, *IEEE Signal Processing Magazine*, 2017, Vol. 34 No..6, pp 85-95, DOI: 10.1109/MSP.2017.2739299.

[17] Jia Yangqing, Shelhamer Evan, Donahue Jeff, Karayev Sergey, Long Jonathan, Girshick Ross,

ISSN: 1992-8645 www.jatit.org E-ISSN: 1817-3195

Guadarrama Sergio, and Darrell Trevor, "Caffe: Convolutional Architecture for Fast Feature Embedding", *In Proceedings of the 22nd ACM international conference on Multimedia (MM '14). Association for Computing Machinery, New York, NY, USA*, November 2014, pp 675–678. DOI: https://doi.org/10.1145/2647868.2654889

[18] T. Chen, M. Li, Y. Li, M. Lin, N. Wang, M. Wang, T. Xiao, B. Xu, C. Zhang, and Z. Zhang, "MXNet: A Flexible and Efficient Machine Learning Library for Heterogeneous Distributed Systems". *CoRR*, 2015, abs/1512.01274.

[19] M. Abadi, P. Barham, J. Chen, Z. Chen, A. Davis, J. Dean, M. Devin, S. Ghemawat, G. Irving, M. Isard, others, "TensorFlow: A System for Large-Scale Machine Learning". *OSDI*, 2016. pp 265-283.

[20] Y. LeCun, Y. Bengio, and G. Hinton, "Deep Learning. Nature", 2015. 521, pp 436-444. DOI: http://dx.doi.org/10.1038/nature14539

[21] K. Nasrollahi, and T.B. Moeslund, "Super-resolution: a comprehensive survey", *Machine Vision and Applications*, 2014, Vol 25, pp 1423–1468. DOI: https://doi.org/10.1007/s00138-014-0623-4.

[22] S. Farsiu, M.D. Robinson, M. Elad, and P. Milanfar, "Fast and robust multi frame super resolution", *IEEE Transactions on Image Processing*, 2004. Vol. 13 No.10, pp 1327-1344, DOI: 10.1109/TIP.2004.834669.

[23] S. P. Belekos, N.P. Galatsanos, and A.K. Katsaggelos, "Maximum a Posteriori Video Super-Resolution Using a New Multichannel Image Prior", *IEEE Transactions on Image Processing,* 2010, Vol. 19 No. 6, pp 1451-146. DOI:10.1109/TIP.2010.2042115.

[24] C. Ledig et al , "Photo-Realistic Single Image Super-Resolution Using a Generative Adversarial Network", *IEEE Conference on Computer Vision and Pattern Recognition (CVPR), Honolulu, HI, USA*, July 2017, pp 105-114. DOI: 10.1109/CVPR.2017.19.

[25] W. S. Lai, J.B. Huang, N. Ahuja, and M.H. Yang, "Fast and Accurate Image Super-Resolution with Deep Laplacian Pyramid Networks", *IEEE Transactions on Pattern Analysis and Machine Intelligence*, 2018. Vol. 41 No. 11, pp 2599-2613. DOI:10.1109/TPAMI.2018.2865304.

[26] R. Sustika, A.B. Suksmono, D. Danudirdjo, and K. Wikantika, "Generative Adversarial Network with Residual Dense Generator for Remote Sensing Image Super Resolution", *International Conference on Radar, Antenna, Microwave, Electronics, and Telecommunications (ICRAMET), Tangerang, Indonesia,* November 2020,. pp 34-39, DOI: 10.1109/ICRAMET51080.2020.9298648.

[27] J. Zhao, Z. Chen, C. Liu, Y. Yang, M. Ye, and Y. Zhang, "Single Image Super-Resolution Based on Enhanced Residual Neural Network", *14th International Conference on Signal Processing Systems (ICSPS), Jiangsu, China*, November 2022, pp 798-803. DOI: 10.1109/ICSPS58776.2022.00145.

[28] P. K. Sahoo, M. K. Nanda, and J. Mohammed, "A Modified Framework for Reversible Digital Image Watermarking", *International Conference on Applied Machine Learning (ICAML), Bhubaneswar, India*, 2019, pp 228-234. DOI: 10.1109/ICAML48257.2019.00049.

[29] J. Krislynd, S. Aprianto, and D. Suhartono, "A comparative study of various convolutional neural network architectures for eye tracking system", *Journal of Image and Graphics*, 2022, Vol. 10 No. 4, pp 178–183. DOI: 10.18178/joig.10.4.178-183.

[30] C. Liu, W. Freeman, R. Szeliski et al., "Noise estimation from a single image", *IEEE Computer. Society. Conference on Computer Vision and Pattern Recognition*, July 2006,Vol 1, pp 901–908. DOI: 10.1109/CVPR.2006.207

[31] A. S. Panayides et al., "AI in Medical Imaging Informatics: Current Challenges and Future Directions", *IEEE Journal of Biomedical and Health Informatics*, 2020, Vol. 24 No. 7, 1837-1857, DOI: 10.1109/JBHI.2020.2991043.

[32] Baidaa Mutasher Rashed, Popescu Nirvana, "Critical Analysis of the Current Medical Image-Based Processing Techniques for Automatic Disease Evaluation" *Systematic Literature Review. Sensors (Basel, Switzerland)*, 2022, Vol. 22 No. 18, pp 7065. DOI:10.3390/s22187065.

[33] P. H. Dinh, "An improved medical image synthesis approach based on marine predators algorithm and maximum gabor energy" *Neural Computing and Applications*, 2022, Vol. 34, No. 6, pp 4367–4385.

[34] D. Patil *et al*., "Medical image segmentation: a review". *International Journal of Computer Science and Mobile Computing,* 2013, Vol. 2 No. 1, pp 22-27.

[35] E. Miranda, M. Aryuni, and E. Irwansyah, "A survey of medical image classification techniques", *International Conference on Information Management and Technology (ICIMTech), Bandung, Indonesia*, November 2016, pp 56-61, DOI: 10.1109/ICIMTech.2016.7930302.

[36] S. Q. Nisa, A.R. Ismail, M.A.B.M. Ali and M.S. Khan, "Medical Image Analysis using Deep Learning: A Review", *IEEE 7th International Conference on Engineering Technologies and Applied Sciences (ICETAS), Kuala Lumpur, Malaysia,* December 2020, pp 1-3. DOI: 10.1109/ICETAS51660.2020.9484287.

[37] Monika A Myszczynska, et al., "Applications of machine learning to diagnosis and treatment of neurodegenerative diseases", *Nature reviews. Neurology,* 2020, (2020). Vol. 16 No. 8, pp 440-456. DOI: 10.1038/s41582-020-0377-8.

[38] T. Guruswamy, L. Gades, A. Miceli, U. Patel, and O. Quaranta, "Beamline Spectroscopy of Integrated Circuits with Hard X-Ray Transition Edge Sensors at the Advanced Photon Source", *IEEE Transactions on Applied Superconductivity*, 2021, Vol. 31 No. 5, pp 1-5, 2101605. DOI: 10.1109/TASC.2021.3067246.

[39] M. F. Ahmed, S. Yasar, and S.H. Cho, "A Monte Carlo Model of a Benchtop X-Ray Fluorescence Computed Tomography System and Its Application to Validate a Deconvolution-Based X-Ray Fluorescence Signal Extraction Method", *IEEE Transactions on Medical Imaging*, 2018, Vol. 37 No. 11, pp 2483-2492, DOI: 10.1109/TMI.2018.2836973.

[40] P. Urbański, M. Białas, M. Krysztof, and T. Grzebyk, "Transmission Target for a MEMS X-Ray Source", *Journal of Microelectromechanical Systems*, 2023, Vol. 32, No. 4, pp. 398-404. DOI: 10.1109/JMEMS.2023.3283536.

[41] R. Hosch, M. Weber, M. Sraieb, et al., "Artificial intelligence guided enhancement of digital PET: Scans as fast as CT?" *European Journal of Nuclear Medicine and Molecular Imaging*, 2022, Vol 49, pp 4503–4515.

[42] P. Kellman, and E. McVeigh, "Image reconstruction in SNR units: A general method for SNR measurement", *Magnetic Resonance in Medicine*, 2005, Vol. 54 No. 6, pp 1439–1447. DOI: 10.1002/mrm.20713.

[43] M. Vangu, and J. Momodu, "F-18 FDG PET/CT Imaging in Normal Variants, Pitfalls and Artifacts in the Abdomen and Pelvis", *Frontiers in Nuclear Medicine*, 2022, Vol. 1, pp 1–12. DOI: 10.3389/fnume.2021.826109.

[44] A. Trequattrini, S. Besio, S. Pittaluga, V. Punzo, and L. Satragno, "A Novel 0.25 T Dedicated MRI Apparatus", *IEEE Transactions on Applied Superconductivity*, 2006, Vol. 16, No. 2, pp 1505-1508. DOI: 10.1109/TASC.2006.871341.

[45] J. Fang et al., "Design of superconducting MRI surface coil by using method of moment", *IEEE Transactions on Applied Superconductivity*, 2002,.Vol. 12, No. 2, pp 1823-1827. DOI: 10.1109/TASC.2002.1020344.

[46] S. Besio, S. Pittaluga, V. Punzo, and A. Trequattrini, "Elliptical Coils for Dedicated MRI Magnets, *IEEE Transactions on Applied Superconductivity,*, 2008. Vol. 18, No. 2, pp 908-911. DOI: 10.1109/TASC.2008.922275.

[47] J. Franke et al., "System Characterization of a Highly Integrated Preclinical Hybrid MPI-MRI Scanner", *IEEE Transactions on Medical Imaging,* 2016, Vol. 35, No. 9, pp 1993-2004. DOI: 10.1109/TMI.2016.2542041.

[48] K. H. Lee et al., "Performance of large-size Superconducting coil in 0.21T MRI system", *IEEE Transactions on Biomedical Engineering,* 2004, Vol. 51, No. 11, pp 2024-2030. DOI: 10.1109/TBME.2004.831539.

[49] A. Geissler, A. Gartus, T. Foki et al., "Contrast-to-Noise Ratio (CNR) as a quality parameter in fMRI", *Journal of Magnetic Resonance Imaging,* 2007, Vol. 25, No. 6, pp 1263–1270. DOI: 10.1002/jmri.20935.

[50] A. J. Morahan et al., "Challenges in Acquiring Clinical Simultaneous SPECT-MRI on a PET-MRI Scanner", *IEEE Transactions on Radiation and Plasma Medical Sciences*, 2023, Vol. 7, No. 7, pp 755-763. DOI: 10.1109/TRPMS.2023.3287639.

[51] M. Watanabe, K. Kawai-Miyake, Y. Fushimi et al., "Application of a flexible PET scanner combined with 3 T MRI using non-local means reconstruction: Qualitative and quantitative comparison with whole-body PET/CT", *Molecular imaging and biology*, 2022, Vol. 24, No. 1, pp 167– 176. DOI:10.1007/s11307-021-01651-8.

[52] Y. Wang, S.H. Huang, M. Feng, and Y. Chen, "Simultaneous Subsea Gas Plumes Detection

and Positioning Using a Transceiver of an Ultra-Short Baseline System", *IEEE Sensors Journal*, 2022, Vol. 22, No. 6, pp 5778-5786. DOI: 10.1109/JSEN.2022.3146268.

[53] A. Lubna, S. Kalady, and A. Lijiya, "MoBVQA: A Modality based Medical Image Visual Question Answering System", *TENCON 2019 - 2019 IEEE Region 10 Conference (TENCON), Kochi, India,* October 2019, pp 727-732. DOI: 10.1109/TENCON.2019.8929456.

[54] M. Ljungberg, and K. S. Gleisner, "3-D Image-Based Dosimetry in Radionuclide Therapy", *IEEE Transactions on Radiation and Plasma Medical Sciences*, 2018, Vol. 2, No. 6, pp 527-540. DOI: 10.1109/TRPMS.2018.2860563.

[55] A. Mehranian, S.D. Wollenweber, M.D. Walker et al., "Image enhancement of whole-body oncology [18F]-FDG PET scans using deep neural networks to reduce noise", *European Journal of Nuclear Medicine and Molecular Imaging*. 2022, Vol. 49, No. 2, pp 539–549. DOI: 10.1007/s00259- 021-05478-x.

[56] R. Boellaard, R. Delgado-Bolton, and W.J.G. Oyen, "FDG PET/CT: EANM procedure guidelines for tumor imaging: Version 2.0", *European Journal of Nuclear Medicine and Molecular Imaging, Springer,* 2015, Vol. 42 No. 2, pp 328–354. DOI: 10.1007/s00259-014-2961-x.

[57] Z. T. Al-Sharify, T.A. Al-Sharify, N.T. Al-Sharify et al., "A critical review on medical imaging techniques (CT and PET scans) in the medical field", *IOP Conference Series: Materials Science and Engineering,* June 2020, Vol. 870, No. 1, DOI: 10.1088/1757- 899X/870/1/012043.

[58] S. Afshari, A. BenTaieb, and G. Hamarneh, "Automatic localization of normal active organs in 3D PET scans", *Computerized Medical Imaging Graphics,* 2018, Vol. 70, pp 111–118. DOI: 10.1016/j.compmedimag.2018.09.008.

[59] C. I. Lee, A.H. Haims, E.P. Monico et al., "Diagnostic CT scans: Assessment of patient, physician, and radiologist awareness of radiation dose and possible risks", *Radiology*, 2004, Vol. 231, No. 2, pp 393–398. DOI: 10.1148/radiol.2312030767.

[60] J. Cui, K. Gong, N. Guo et al., "PET image denoising using unsupervised deep learning", *European. Journal of Nuclear Medicine and Molecular Imaging*, 2019, Vol. 46, No. 13, pp 2780–2789.

[61] S. Kaviani, M. Mokri, C. Cohalan et al., "Quality enhancement of dynamic brain PET images via unsupervised learning", *13th Biomedical Engineering International Conference, Ayutthaya, Thailand,* November 2021, pp 1–4, DOI:10.1109/BMEiCON53485.2021.9745248.

[62] D. W. Townsend, J.P.J. Carney, J.T. Yap et al., "PET/CT today and tomorrow", *Journal of nuclear medicine: official publication, Society of Nuclear Medicine*, 2004, Vol. 45, No. 1, pp 4-14. DOI: 10.3833/pdr.v2100i9999.7.

[63] B. M. Rashed, and N. Popescu, "Critical Analysis of the Current Medical Image-Based Processing Techniques for Automatic Disease Evaluation: Systematic Literature Review", *Sensors*, 2022, Vol. 22, No. 18, 7065. DOI: 10.3390/s22187065.

[64] Bevilacqua, Marco et al., "Low-Complexity Single-Image Super-Resolution based on Nonnegative Neighbor Embedding", *British Machine Vision Conference (BMVC),* November 2012, pp 1-10. DOI:10.5244/C.26.135.

[65] R. Zeyde, M. Elad, and M. Protter, "On Single Image Scale-Up Using Sparse-Representations": *Boissonnat,* JD., et al. "Curves and Surfaces. Curves and Surfaces" *Lecture Notes in Computer Science,* 2010, *6920. Springer, Berlin, Heidelberg.* November 2010, DOI: 10.1007/978-3-642-27413-8_47.

[66] Z. Xu, M. Gao, G. Papadakis et al., "Joint solution for PET image segmentation, denoising, and partial volume correction", *Medical Image Analysis*, 2018, Vol. 46, pp 229–243. DOI: 10.1016/j.media.2018.03.007.

[67] A. Vijayvargiya, R. Kumar, N. Dey and J.M.R.S. Tavares, "Comparative Analysis of Machine Learning Techniques for the Classification of Knee Abnormality", *IEEE 5th International Conference on Computing Communication and Automation (ICCCA), Greater Noida, India*, October 2020, pp 1-6, DOI: 10.1109/ICCCA49541.2020.9250799.

[68] P. H. Dinh and N. L, "Giang A new medical image enhancement algorithm using adaptive parameters", *International Journal of Imaging Systems and Technology*, 2022,Vol. 32, No. 6, pp 2198–2218. DOI:10.1002/ima.22778.

[69] S. Savvin, and A. Sirota, "An Algorithm for Multi-Fame Image Super-Resolution under Applicative Noise Based on a Convolutional Neural Network", *2nd International Conference*

on Control Systems, Mathematical Modeling, Automation and Energy Efficiency (SUMMA), Lipetsk, Russia, November 2020, pp 422-424, DOI: 10.1109/SUMMA50634.2020.9280698.

[70] B. Gerges, W. Li, M. Leonardi, B.W. Mol, and G. Condous, "Optimal imaging modality for detection of rectosigmoid deep endometriosis: systematic review and meta-analysis", *the official journal of the International Society of Ultrasound in Obstetrics and Gynecology*, 2021, Vol. 58, No. 2, pp 190-200. DOI: 10.1002/uog.23148.

[71] YiNan Zhang, and MingQiang, "An Deep Learning- and Transfer Learning-Based Super Resolution Reconstruction from Single Medical Image", *Journal of Healthcare Engineering,* 2017, 5859727. DOI:10.1155/2017/5859727.

[72] J. Lemley, S. Bazrafkan, and P. Corcoran, "Smart Augmentation Learning an Optimal Data Augmentation Strategy", *IEEE Access*, Vol. 5, pp 5858-5869. DOI: 10.1109/ACCESS.2017.2696121.

[73] H.C. Shin, et al., "Medical Image Synthesis for Data Augmentation and Anonymization Using Generative Adversarial Networks", A. Gooya, O. Goksel, I. Oguz, N. Burgos, (eds) *Simulation and Synthesis in Medical Imaging. SASHIMI 2018. Lecture Notes in Computer Science, 11037, Springer, Cham.,* 2018, DOI: 10.1007/978-3-030-00536-8_1.

[74] Ekin D. Cubuk, et al., "Autoaugment: Learning augmentation policies", *from data. Computer Vision and Pattern Recognition, arXiv preprint arXiv:* 1805.09501. 2024, DOI: https:10.48550/arXiv.1805.09501.

[75] B. Zoph, V. Vasudevan, J. Shlens, and Q.V. Le, "Learning Transferable Architectures for Scalable Image Recognition", *2018 IEEE/CVF Conference on Computer Vision and Pattern Recognition, Salt Lake City, UT, USA,* June, 2018, pp 8697-8710. DOI: 10.1109/CVPR.2018.00907.

[76] Y. Liang, J. Wang, S. Zhou, Y. Gong, and N. Zheng, "Incorporating image priors with deep convolutional neural networks for image super-resolution", *Neurocomputing*, 2016, Vol. 194, pp 340-347, DOI: 10.1016/j.neucom.2016.02.046.

[77] J. Lehtinen, et al. (2024), "Noise2Noise: Learning image restoration without clean data. Computer Vision and Pattern Recognition", *arXiv preprint arXiv*:1803.04189. DOI:10.48550/arXiv.1803.04189.

[78] S. Borman, R. L. Stevenson, "Super-resolution from image sequences-a review", *Midwest Symposium on Circuits and Systems (Cat. No. 98CB36268), Notre Dame, IN, USA,* August 1998, pp 374-378. DOI:10.1109/MWSCAS.1998.759509.

[79] N. K. Bose, H.C. Kim, and B. Zhou, "Performance analysis of the TLS algorithm for image reconstruction from a sequence of under sampled noisy and blurred frames", *1st International Conference on Image Processing, Austin, TX, USA*, November 1994, Vol. 3, pp 571-574. DOI: 10.1109/ICIP.1994.413741.

[80] W. B. Lim, M.K. Park, and M. G. Kang, "Spatially adaptive regularized iterative high-resolution image reconstruction algorithm", *Proceeding of SPIE Visual Communications and Image Processing*, January 2001, 4310. DOI:10.1117/12.411797.

[81] N. Nguyen, P. Milanfar, and G. Golub, "Efficient generalized cross-validation with applications to parametric image restoration and resolution enhancement", *IEEE Transactions on Image Processing,* 2001, Vol, 10, No. 9, pp 1299-1308. DOI: 10.1109/83.941854.

[82] N. Nguyen, P. Milanfar, and G. Golub, "A computationally efficient super resolution image reconstruction algorithm". *IEEE Transactions on Image Processing,* 2001, Vol. 10, No. 4, pp 573-583. DOI: 10.1109/83.913592.

[83] M. Elad, and Y. Hel-Or, "A fast super-resolution reconstruction algorithm for pure translational motion and common space-invariant blur", *IEEE Transactions on Image Processing*, 2001, Vol. 10, No. 8, pp 1187-1193, DOI: 10.1109/83.935034.

[84] P. K. Sahoo, and M. K. Nanda, "A modified partitioning algorithm for classification of e-waste", *Journal of Statistics and Management Systems,* 2023, Vol. 26, No. 1, pp 53-65. DOI: 10.47974/JSMS-947

[85] D. Gountia and S. Roy, "Security Model for Protecting Intellectual Property of State-of-the-Art Microfluidic Biochips", *Elsevier Journal on Information Security and Applications (JISA),* 2021,Vol. 58: pp 1-15.

[86] P.K. Sahoo, D Gountia,., R.K Dash,., S. Behera, and M.K. Nanda, "An Extension Application of 1D Wavelet Denoising Method for Image

Denoising",. *In: Lanka, S., Sarasa-Cabezuelo, A., Tugui, A. (eds) Trends in Sustainable Computing and Machine Intelligence. ICTSM 2023. Algorithms for Intelligent Systems. Springer, Singapore*, (2024).. https://doi.org/10.1007/978-981-99-9436-6_7